UCRL8754

UNIVERSITY OF
CALIFORNIA

Ernest O. Lawrence

Radiation Laboratory

PRODUCTION AND DECAY OF THE K^0 MESON

BERKELEY, CALIFORNIA

DISCLAIMER

UCRL-8754
Physics and
Mathematics

UNIVERSITY OF CALIFORNIA
Lawrence Radiation Laboratory
Berkeley, California

Contract No. W-7405-eng-48

PRODUCTION AND DECAY OF THE K^0 MESON

Sherwood Parker

(Thesis)

May 18, 1959

Printed for the U. S. Atomic Energy Commission

Printed in USA. Price $2.25. Available from the
Office of Technical Services
U. S. Department of Commerce
Washington 25, D. C.

PRODUCTION AND DECAY OF THE K^0 MESON

Contents

PRODUCTION AND DECAY OF THE K^0 MESON

Sherwood Parker

Lawrence Radiation Laboratory
University of California
Berkeley, California

May 18, 1959

ABSTRACT

The production and decay of strange particles have been studied by observing the space around a Bevatron target with a well-collimated gamma detector. Strange particles that have π^0 modes of decay can send gammas up to the detector from the subsequent decay of the π^0. The observed-gamma counting rate as a function of the detector and collimation position was then compared with that predicted for various assumptions about the production matrix element.

The data require contributions to the counting rate from two known decay modes, $K^0 \rightarrow \pi^0 + \pi^0$ and $K^{\pm} \rightarrow \pi^{\pm} + \pi^0$, $\pi^0 \rightarrow \gamma + \gamma$. It is also consistent with limited contributions from $\Lambda^0 \rightarrow \pi^0 + n$, $\Sigma^+ \rightarrow \pi^0 + p$, $\Sigma^0 \rightarrow \Lambda^0 + \gamma$, $\Lambda^0 \rightarrow \pi^0 + n$, but cannot give any information about these decays. The observed angular distribution requires that a significant part of the K^0 production be sharply peaked at high energies and at angles close to the line of collision of the incoming nuclei. The peaked part of the angular distribution can be fitted by $\cos^k\theta_{Kc}$, where θ_{Kc} is the polar angle of the K particle in the center of momentum system, and we have $k \geq 8$, with the best fits for $k = 12$ to 16.

I. INTRODUCTION

Despite the large number of particles having lifetimes of the order of 10^{-8} to 10^{-10} seconds, only one meson, the K^0, has a reasonable probability of being produced and then decaying within several centimeters of a target bombarded with 6-Bev protons. Furthermore, all other particles having similar life times-- the Λ, Σ, Ξ hyperons-- are restricted to laboratory angles of 75 degrees or less from the beam direction, because of their greater mass and consequent slower velocities in the center-of-momentum (c. m.) system. Thus observations of decay products originating alongside of or upstream from a Bevatron target and within several centimeters of it can give us information about the production and decay of the K^0 meson.

Consider the region around a target bombarded with high-energy protons. Pions in all directions and scattered protons in the downstream hemisphere will come off in great numbers. In order to detect strange particles unambiguously without using a mass determination, it is necessary to shield the detector from the direct target radiation and use the fact that the strange particles can "turn corners" by way of their decay products. The region to either side and upstream from the target and within several cm of it will be traversed by $e^{\pm}$, $\mu^{\pm}$, $\pi^{\pm}$, $K^{\pm}$, K^0_2, and K^0_1 particles (in addition to the beam protons). The $\mu^{\pm}$ has an insignificant probability of decaying. The $\pi^{\pm}$ has a larger though still small probability of decaying, but does not have enough "Q" to let its decay μ come off at an appreciable angle to its flight path. The $K^{\pm}$ has a decay probability somewhat larger than the π, and when it decays it can send a $\pi^{\pm}$, $\mu^{\pm}$, $e^{\pm}$, or a γ (from the decay π^0) in the direction of the detector. The K^0_2-decay probability is again small enough to neglect. The K^0_1 on the other hand, has a high decay probability and a high Q, and can with a relatively large probability ($\sim$ 20 times that of a $K^{\pm}$) send to a detector a $\pi^{\pm}$ from its charged decay mode or one or two gammas of the four created from neutral pions in its neutral decay mode.

In addition to the above particles, Λ, Σ, and Ξ hyperons will be able to send decay products to a detector viewing regions downstream from the target. Because of less favorable kinematics because of their heavier masses and lower Q values, they will be perhaps only about 10% as efficient as the K^0_1 in sending decay products to a detector.

Thus a detector of high-energy γ rays looking at nearby regions upstream from a target will see gammas from $K^0_1 \rightarrow \pi^0 + \pi^0$ and $K^{\pm} \rightarrow \pi^{\pm} + \pi^0$, $\pi^0 \rightarrow \gamma + \gamma$ (the K^+ with less probability and the K^- with far less probability because of its smaller production cross section). Looking downstream it will see also those from $\Lambda^0 \rightarrow n + \pi^0$ and $\Sigma^+ \rightarrow p + \pi^0$, $\pi^0 \rightarrow \gamma + \gamma$. These γ rays for the most part come from particles that headed upstream in the c. m. system and were projected forward in the laboratory. A particle going downstream in the c. m. system is moving rapidly enough in the laboratory to Doppler shift any γ rays coming out at right angles to relatively low energies.

A detector of high-energy charged particles similarly will see pions from $K^0_1 \rightarrow \pi^+ + \pi^-$, a smaller number of charged particles from $K^{\pm} \rightarrow \mu^{\pm} + \nu$ and $\pi^{\pm} + \pi^0$ upstream, and these together with pions from $\Lambda^0 \rightarrow p + \pi^-$ and $\Sigma^{\pm} \rightarrow n + \pi^{\pm}$ downstream. In addition to some detailed information on the production of K^0 mesons a comparison with the results of the gamma detector may give some idea of the branching ratio of the K^0_1.

Because of the lack of an external proton beam at the Bevatron and because of the short decay distances of the particles involved, it is necessary to place the detectors close to the Bevatron. The necessity of selecting particles originating only a few centimeters from the target and not those from the target made it imperative that the detector be well collimated and thus have a small solid angle. This makes a coincidence experiment in which two decay products are detected very difficult because of the low counting rate that two well-collimated detectors would have.

A number of experiments studying γ rays originating in the space near a target have been carried out. The principle was used by

Bjorklund, Crandall, Moyer, and York[1] to set an early upper limit on the π^0 lifetime; by Garwin[2] and Balandin et al.[3] in a search for strange particles at a proton energy that has since proved to be below threshold; by Ridgway, Berley, and Collins[4, 5, 6] at the Brookhaven Cosmotron and by Osher[7, 8, 9] at the Bevatron, the latter two experiments indicating the existence of the decay mode $K^0_1 \rightarrow \pi^0 + \pi^0$. The experiment described here is a continuation of that of Osher et al.[9] Its object is to determine, as well as possible, the production matrix element of the K^0 meson as a function of c.m. polar angle for the K^0 and as a function of the momentum in this system. The experimental work for a continuation of this study using the detection of charged decay products has been completed and will be described in a future report.

II. PHYSICAL SET UP

The experiment was performed at the west tangent tank of the Bevatron (Fig. 1). Directly over a plunging probe that carried the target, a re-entrant well allowed collimation shielding to come within 25 cm. of the target. The bottom of the well contained a 1/2-in. -thick lucite window 6-in. in diameter through which γ rays to be observed could pass (Fig. 2).

The collimation allowed γ rays traveling within about 1^{o} of vertical to reach a counter telescope. Three collimating lead slits were used. Each one was 2 in. thick (10 radiation lengths). The lowest was placed immediately above the lucite window and had the largest opening. The opening was large enough so that none of the collimator was visible from the counter telescope and yet it was small enough so that none of the target was visible from the faces of the second opening. This required any direct radiation from the target to scatter at least twice before reaching the counter, with at least one of the scatters being well outside the forward cone of $\sim 1/2^{o}$ or less into which almost all high-energy pairs and γ rays were produced. (See Fig. 2).

The second and third collimating slits defined the region viewed by the telescope and were bounded by radial lines and segments of concentric circles centered about the vertical line through the center of the target. The 30 radiation lengths of lead in these three shields were enough to degrade essentially all showers originating from target-produced π^{0} mesons to well below the counter threshold of 40 Mev. Neutrons, and pions charge-exchanging to produce π^{0} mesons, can also produce background γ rays. Most pions, having an energy of only several hundred Mev, would be stopped by the 6-in. of lead. However a collision involving a nucleon with maximum Fermi momentum directed upstream could produce a pion of slightly less than 900 Mev traveling upwards. In order to attenuate neutrons and these pions and reduce general background due to multiple scattering from the lower slits, an additional 10-in. of lead was placed between and above these shields.

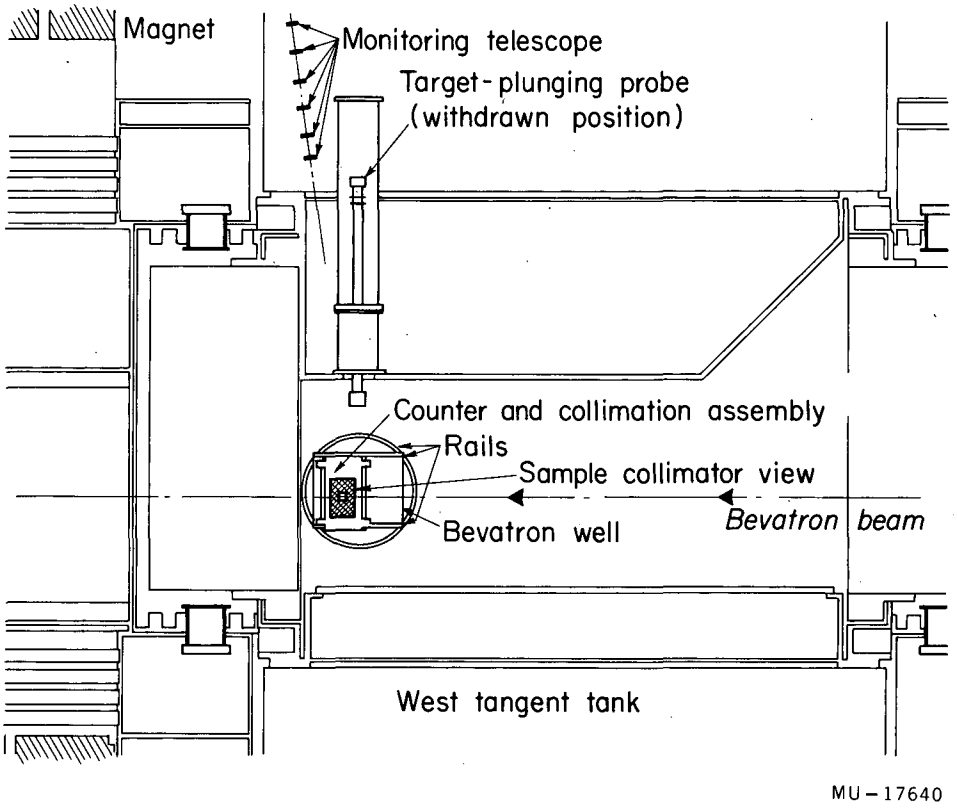

Fig. 1. Plan view of Bevatron west target area showing tangent tank, well, counter, and monitoring telescope.

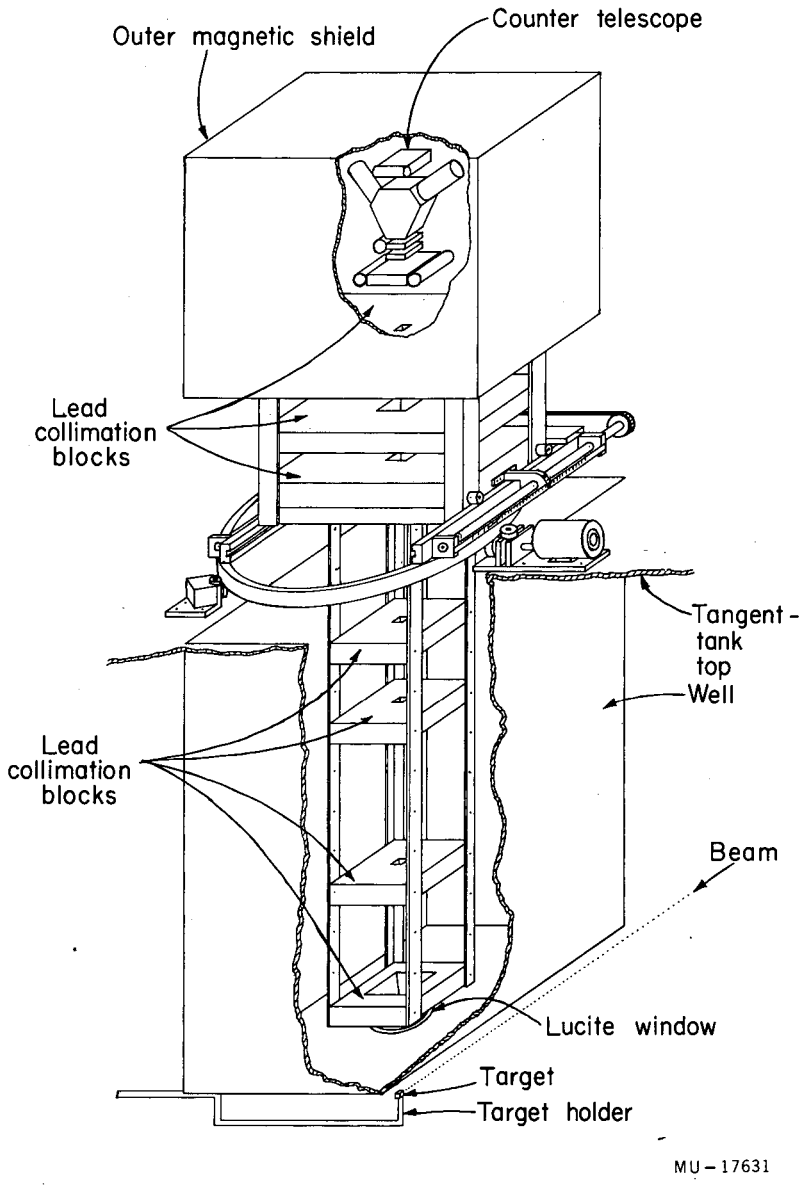

Fig. 2. Counter in tangent-tank well.

The dimensions of the slits (Fig. 3) were:

defining slits for 1-in. radius: 30° angle, 3/4-in. minimum radius, 1-1/4-in. maximum radius.

defining slits for 2-in. radius: $22\text{-}1/2^{\circ}$ angle, 1-1/2-in. minimum radius, 2-1/2-in. maximum radius.

defining slits for 3-in. radius: 15° angle, 2-1/2-in. minimum radius, 3-1/2-in. maximum radius.

lower shielding slit for 1-in. radius: 0.85 (radial) by 1.15 in.

lower shielding slit for 2-in. and 3-in. radii: 1.55 by 1.55 in.

lower shielding slit for background check: no opening.

These dimensions were chosen small enough to detect reasonable detail in the angular distribution. The need for an adequate counting rate and the neutron background put a lower limit on slit size. (Neutron background, being insensitive to slit size, would become relatively important for small slits.)

The entire counter and collimation assembly was mounted on a motor-driven framework that could be rotated about a vertical axis passing through the center of the target and could be moved in and out radially. The three collimating slits could be changed so the sides were always radial lines and segments of concentric circles for each radial setting of the frame. The position of the frame was determined from direct-reading scales viewed by a telescope (optical this time) and a multiple mirror system so changes in position could be made without interrupting the Bevatron operation.

The target was a 1/2-in. cube of tantalum. It was on the end of a horizontal probe that plunged the target into position as the initial beam oscillations died down. In order to keep the beam from striking the more massive probe, it was connected to the target by means of a thin-walled steel tube which was bent first down, then horizontally out to under the target at a level below that of the beam, and then up to support the target from below. The tube had about 5% as much mass per unit length as the target. Any small amount of beam interacting with the support will do so directly below the target and thus will not even be a second-order correction to the observed angular distribution.

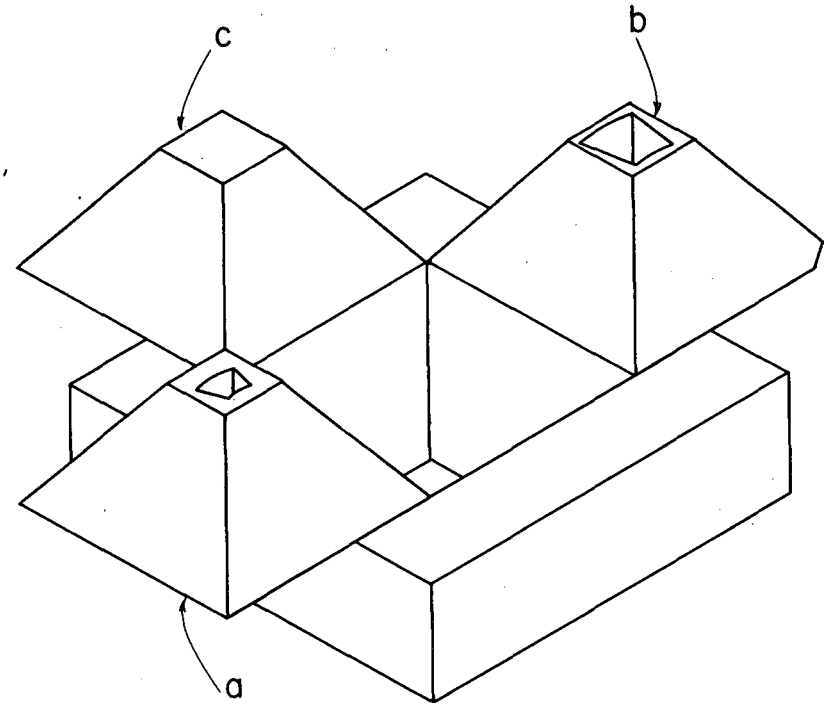

MU-17638

Fig. 3. Collimation doors and base block. (a) Collimator for observations at 1-in. radius; (b) collimator for observations at 2-in. radius; (c) block for background observations.

III. THE COUNTER TELESCOPE

The counter telescope used in the neutral decay mode part of the experiment is essentially the same as that described by Osher[7] (Fig. 4). To count, a γ ray must pass through a 4 by 4 by 1-in. plastic anticoincidence scintillator (last dimension in beam direction) without making a light pulse and convert in a 2 by 2 by 0.196-in. lead converter, with one or both members of the electron-positron pair counting in the following 2 by 2 by 1-in. plastic scintillator (S1), a pentagonal-shaped lucite Cherenkov counter 5 in. thick in the beam direction (Cer), and a final 3-in.-by 3-in. by 1-in. plastic scintillator (S2).

The anticoincidence scintillator was large enough to require all charged particles coming through the slits or scattering from the collimators and passing through S1, the Cherenkov counter, and S2 to also pass through it and thus not register as a γ. The Cherenkov counter required the particle to be relativistic and eliminated spurious counts from almost all protons caused by neutrons. The second scintillator, S2, guaranteed a reasonably uniform pulse height in the Cherenkov counter and raised the threshold of the telescope to 40 Mev by requiring that the electron or positron pass completely through the Cherenkov counter. This threshold gives preference to γ rays originating from K^0 decay over those from hyperon decay and general background.

The scintillators were of standard UCRL composition -- 3% terphenyl scintillator and 0.03% tetraphenyl butadiene wavelength shifter in a polystyrene base -- and gave one photon for each 200 ev energy loss. Their light was collected by RCA 1P21 photomultipliers, two for the anticoincidence counter and one each for S1 and S2. The Cherenkov light was collected by two RCA 6810 photomultipliers (Cer 1 and Cer 2). Because the stray field of the Bevatron at the location of the counters reached 450 gauss, the 1P21 photomultipliers and the lucite Cherenkov counter were placed in double magnetic shields and the 6810's in quadruple shields, and the entire assembly was then enclosed in another magnetic shield. All innermost shields were of mu metal.

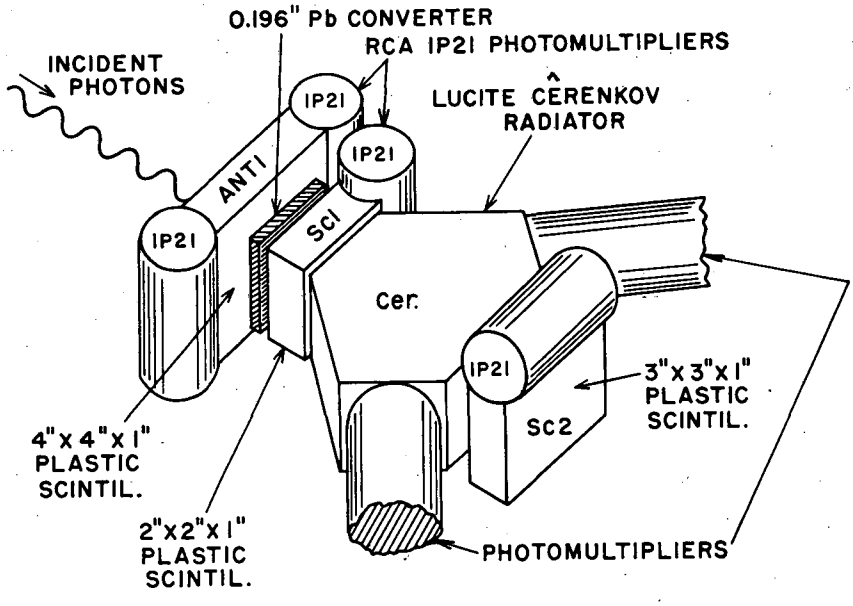

Fig. 4. Gamma telescope.

The lead converter was moved by an electric motor to standard "in" and "out" positions in order to provide data for subtractions from which the γ counting rate is deduced (see page 29).

IV. ELECTRONICS

A block diagram of the electronics is shown in Fig. 5. Pulses from S1 and S2 were amplified in one Hewlett-Packard 460A distributed amplifier each, and those from Cer 1 and Cer 2 in two 460A's each. The pulses were sent to channels 1 through 4 of a Garwin-Wiegand coincidence circuit,[10] and then were terminated. The pulses from the two antiphotomultipliers were added in a passive adder, amplified in two 460A's and sent to channel 5. The signal, with negligible attentuation, was carried through the chassis and through a 1-ft coaxial cable to channel 6 and then terminated. The use of a large antiscintillator, two photomultipliers operated at a relatively high voltage, two amplifiers, and two coincidence-circuit channels are all to insure as high an anti efficiency as possible. Any small remaining inefficiency should be subtracted out when the converter-in–converter-out difference is taken. Channels 1 through 4 went to both of the multiple-coincidence circuits on the chassis (called respectively, the "yes" circuit and the "no" circuit). Channels 5 and 6 went only to the "no" circuit. (A physical connection also existed to the "yes" circuit, but the two input tubes were turned off.) When a γ converted in the converter, only channels 1 through 4 received pulses, so the "yes" circuit gave an output pulse, but the "no" circuit did not. When a charged particle went through the telescope, all channels received pulses, and both the "yes" and "no" circuits gave pulses. These outputs were internally connected to an anticoincidence circuit that gave an output pulse for a "yes" pulse, providing the "no" pulse was absent--the combination resulting from a converting γ. The fast output pulses from the anticoincidence circuit and the "yes" and "no" coincidence circuits were amplified in Hewlett-Packard 460B amplifiers, sent to attenuators for precise control over gain and thus over threshold voltage, and then scaled in Hewlett-Packard prescalers and UCRL 1000 scalers. Shaped scaler outputs were available from the Garwin-Wiegand chassis, but were too slow for this application. The "yes" and "no" outputs were of no direct physical significance but were recorded to check on the operation of the coincidence circuits.

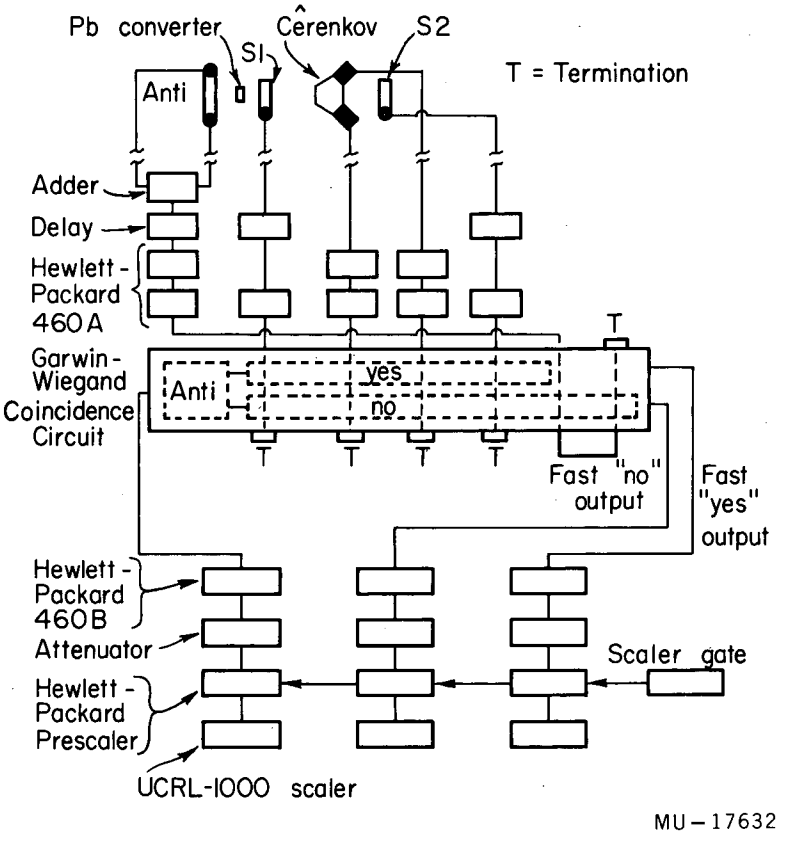

Fig. 5. Electronics block diagram.

The tube voltages, signal-amplifier gains, and output-amplifier gains were plateaued at the beginning of the run. The gains and the coincidence-circuit calibration were checked daily with a millimicrosecond pulse generator.

The resolution time of the coincidence circuit was 10^{-8} sec. Typical counting rates varied from about 10^4 counts per Bevatron beam pulse of 10^{10} protons with the target in the viewed region to about 10 counts per pulse with the target several inches away. The accidental rate was several percent when the counter telescope viewed the target, and was negligible at other times.

V. CALIBRATION OF COUNTER

Before any of the runs, including those described by Osher et al.[7,9] and the one described here, the γ telescope was calibrated at the synchrotron. Since a monoenergetic γ beam of sufficient intensity was not available, the theoretical probability for the creation of an electron or positron of a given energy at a given depth in the lead converter was computed.[11,12] The probability that this electron or positron would count was determined experimentally by directing a beam of monoenergetic electrons on various parts of a 2-by 2-in. piece of lead behind which was placed the rest of the telescope--S1, Cer, and S2. (See Fig. 6). The energy of the electrons was varied from 40 to 300 Mev, and the thickness of the lead was varied from 0 to 1/4 in., simulating electrons of those energies being created at various depths in the converter. The only difference between the electrons in the beam and those created by pair production is a possible difference in their angular spread about the beam line of the counter, but both of these angles were negligible compared with that subtended by the counter at the surface of the lead.

The electrons were made by pair production from the bremmstrahlung beam of the synchrotron. The energy of the beam was analyzed by a pair magnet with lead slits for coarse energy selection and a two-fold counter telescope for fine selection. The scintillators were each 2/3 by 2/3 in. The two-fold telescope, the back counter of which was immediately in front of the 2-by 2-in. piece of lead, also acted as a monitor of those particles impinging perpendicularly on the desired part of the lead.

The two monitor signals went to the first two channels of a Garwin-Wiegand six-fold coincidence circuit and then to a separate two-fold coincidence circuit mounted on the same chassis. The signals from S1, Cer 1, Cer 2, and S2 went to the other four channels of the six-fold circuit. The desired electron efficiency was then ϵ = number of 6-fold counts/number of 2-fold counts. A weighted average of this efficiency for different positions of the two-fold counter telescope gave the average probability for the entire piece of

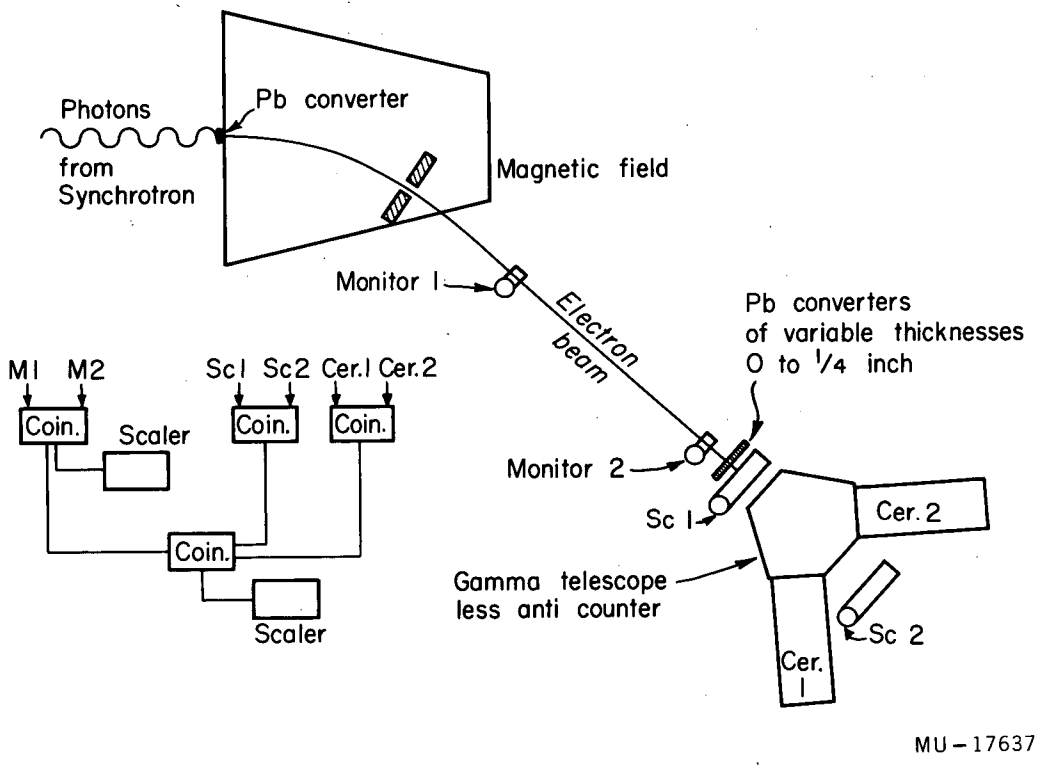

Fig. 6. Gamma-telescope calibration layout.

lead of that thickness ($\equiv t$). This probability $\epsilon(E_-, t)$ plus the probability that the positron will count $\epsilon(E_+, t) = \epsilon(E_\gamma - E_-, t)$ minus the probability that both will count $\epsilon(E_-, t)\epsilon(E_\gamma - E_-, t)$ gives the probability that the converting γ will produce a count.

The pair-production cross section corrected for deviations from the Born approximation, production in the fields of the atomic electrons, and screening is:

$$\sigma(E\gamma, E_\pm)dE_\pm = 2\alpha r_e^2 Z(Z+0.8)\, G(E\gamma, v)\, (dE_\pm/E\gamma),$$

where

$$\alpha = \frac{e^2}{hc}, \quad r_e = \frac{e^2}{mc^2}, \quad v = \frac{E_\pm}{E\gamma}, \text{ and } \gamma = \frac{100\, mc^2}{E\gamma\, v\, (1-v)}\, Z^{-1/3}.$$

For $\gamma >> 1$ (no screening), we have

$$G(E\gamma, v) = [v^2 + (1-v)^2 + 2/3\, v(1-v)]\ [2 \ln \{\frac{2Ev}{mc^2}\, v\, (1-v)\} - 1 - \epsilon(Z)].$$

For $15 \geq \gamma \geq 2$ (intermediate screening), we have

$$G(E\gamma, v) = [v^2 + (1-v)^2 + 2/3\, v(1-v)]\ [2 \ln \{\frac{2E}{mc^2}\, v(1-v)\} - 1 - \epsilon(Z) - 2c(\gamma)].$$

For $2 \geq \gamma \geq 0$ (intermediate screening), we have

$$G(E\gamma, v) = [v^2 + (1-v)^2][\frac{f_1(\gamma)}{2} - 2/3 \ln Z - \epsilon(Z)]$$

$$+ 2/3\, v(1-v)[\frac{f_2(\gamma)}{2} - 2/3 \ln Z - \epsilon(Z)].$$

For $\gamma \cong 0$ (complete screening), we have

$$G(E\gamma, v) = [v^2 + (1-v)^2 + 2/3\, v(1-v)]\ [2 \ln(183 Z^{-1/3}) - \epsilon(Z)] - 2/9\, v(1-v).$$

Here numerical values $f_1(\gamma)$, $f_2(\gamma)$, and $c(\gamma)$ are given in Rossi and range from

$f_1(0) = 20.9$, $f_2(0) = 20.2$, $C(2) = 0.21$ to $f_1(2) = f_2(2) = 15.7$, $C(15) = 0.01$.[12]

The correction to the Born approximation, $\epsilon(Z)$, is 0.67 for lead.

The above formulas are used to find the total pair-production cross section from which the probability of the γ surviving to a given depth T-t in the converter is calculated. Here we define T ≡ converter thickness and t ≡ residual converter thickness to be penetrated by electron. This probability is multiplied by the probability that the electron will have an energy $E_- = \sigma(E\gamma, E_-) \frac{N}{A} dE_- dt$(dt in gm/cm^2) and the probability that a count will result. The resulting expression,

$$\left\{ e^{-\frac{N}{A}[T-t]\sigma_{tot}(E_\gamma)} \right\} \left\{ \epsilon(E_-, t) + \epsilon(E_\gamma - E_-, t) - \epsilon(E_-, t)\,\epsilon(E_\gamma - E_-, t) \right\}$$

$$\times \left\{ \sigma(E_\gamma, E_-) \frac{N}{A} \right\} dE_- dt,$$

is then numerically integrated over E_- and t.

Because the maximum γ energy is 775 Mev, the curves for experimental counting efficiency were extrapolated from the highest measured point at 300 Mev. This does not cause too much error because above 150 Mev the curves have very low curvature and for small t are already above 0.8 at 300 Mev.

The absolute error is estimated to be ~ 15% with major contributions coming from the determination of $\epsilon(E_-, t)$ and the extension of it to 775 Mev. The shape of the efficiency curve (relative efficiency as a function of Eγ) should be known to within about 5%, and it, rather than the absolute efficiency, determines the angular and energy dependence of the production matrix element for the K^0.

The efficiency curve is shown in Fig. 7.

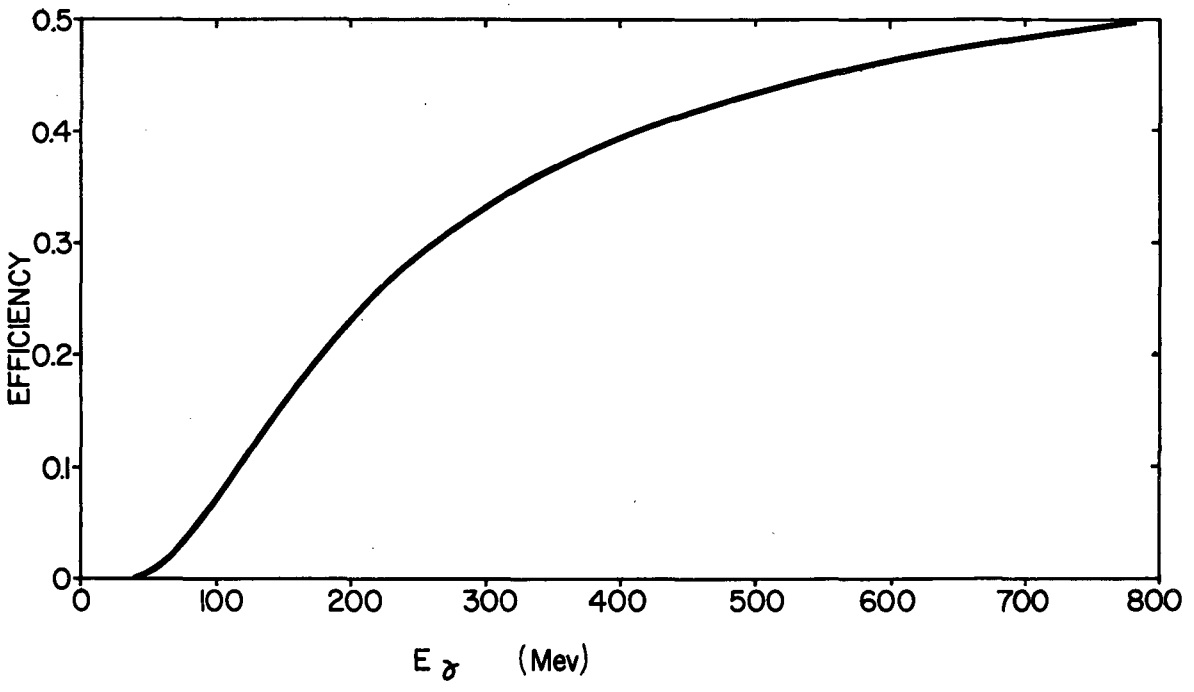

Fig. 7. Gamma-telescope efficiency as a function of gamma energy for normally incident gammas.

VI. THE BEAM

The beam was spilled on the target for 65 msec to keep the accidental rate low and yet permit the use of reasonably large total beams ($\sim 2 \times 10^{10}$ protons/pulse). This caused a spread in beam energy from 6.0 to 6.2 Bev. The spread in c. m. velocity, and energy in the center of momentum caused by the beam-energy spread was small, however, compared with that caused by the internal momenta of the nucleons.

When the target was plunged in the west tangent tank, a large copper block in the east tangent tank was plunged to within several inches of the main target's radius. The beam that struck the target was degraded sufficiently to hit the clipper which further degraded it so that it went into the inside wall.

Three methods were used for monitoring the beam. An induction electrode in the south tangent tank gave a value for the circulating beam. The signal amplitude immediately before the spill started was recorded with an electrometer, and the amplitude before and during the spill was displayed on an oscilloscope. The induction electrode was used mainly to check the shape of the spill.

A six-fold pion telescope set at 82° from the forward direction on the inside west platform served as a pulse-to-pulse relative monitor. It did not respond to beam missing the target as the induction electrode did, but was undesirably sensitive to scattered beam that escaped the clipper and hit the inside wall of the tangent tank, producing pions there.

The third method of monitoring used foils placed on the target and provided an absolute calibration for the pion telescope. The foil method has the advantage that it is sensitive only to beam striking the target and in addition it provides a profile of the beam distribution on the target.

Two kinds of foils were used, aluminum (Al) and gold (Au). The reaction in Al is:

$$Al^{27} + p \rightarrow Na^{24} + \text{other reaction products}$$

$$Na^{24} \rightarrow Mg^{24} + \beta^{-} \text{ (1.39 Mev, } T_{1/2} = 15 \text{ hr).}$$

In Au, the reaction is:

$$Au + p \rightarrow Tb^{169} + \text{other reaction products}$$

$$Tb^{169} \rightarrow Eu^{145} + \alpha(3.95\ \text{Mev},\ T_{1/2} = 4.1\ \text{hr}).$$

The cross section at 6.2 Bev for the former reaction is 10.5 mb,[13] and for the latter is 1.0 mb.[14] The Al foil was 0.003-in. thick, was placed upstream from the target, and had 0.001-in. guard foils immediately ahead of and behind it. The guard foil between it and the target stopped recoiling nuclear fragments from the target and combined with the upstream guard foil to send as many recoiling Na^{24} nuclei into the 0.003-in. foil as it lost to them. After waiting at least 20 hr to allow short-lived products to decay, the β particles from Na^{24} were counted with a Geiger counter. The true counting rate was determined from the observed rate by multiplying by the factors listed in Table I. Corrections for the decay of the activity before measuring time and for relative fluctuation in the intensity of the Bevatron beam as seen by one of the other monitors were accounted for by the use of the formula

$$N = C \left[\sum_i r_i T_i \right] \left[\sum_i r_i (1 - e^{-\lambda T_i})\, e^{-\lambda t_i} \right]^{-1} ,$$

where

N = number of Na^{24} atoms made times branching ratio for β decay

C = β counting rate

$\lambda \equiv$ decay constant

r_i = number proportional to beam intensity from a time $T_i + t_i$ before β counting to a time t_i before β counting

The observed lifetime agreed with the published value within the accuracy of measurement. One major source of error remained uncorrected. Recoil neutrons from the target can cause the reaction

$$Al^{27} + n \rightarrow Na^{24} + \alpha .$$

Table I

Correction factors for determination of true beta-counting rate

Correction	Factor
Counter efficiency	1/0.130
Counts from gamma rays	0.970[a]
Back scattering from aluminum tray supporting the foil	0.78
Scattering and absorption in the foil	0.91
Window and air absorption	1.02
Cosmic-ray background	Usually about 0.995 to 0.999
Wall and air scattering	0.00[b]
Dead time	270 μsec recovery time assumed

[a]Factor determined by stopping the beta particles with lead and extrapolating the gamma counting rate back to a no-lead counting rate.

[b]No correction was needed, because the counter shield was lined with Al.

In order to avoid this source of error and provide data for correcting the earlier runs in which only Al foils were used, 0.001-in. Au foils were used in later runs. The beauty of the Au → Tb reaction is that it has a threshold of 600 Mev. Two hours after a bombardment, the 4.1-hr Tb decay is the only one observed. Unlike the Al foils for β counting, a Au foil thin compared with the range of the α particle would be so thin ($\sim 1/3$ mg/cm^2) that it would have to be evaporated on a backing foil and removed from the backing for counting. The backing foil and a guard foil would also have to be counted because recoils out of such a thin foil would be very large (50 to 80%). These difficulties were avoided by using infinitely thick (0.001-in.) Au foils. The downstream face of the foil was always counted. A 0.001-in. Al guard foil was placed between this face and a second Au foil which was used as a check against the first one.

The α activity was counted in an ionization chamber through which methane was flowed. The foil to be counted was placed in a standard position on a tray which slid into place under a horizontal circular collecting electrode. The signal was amplified in a shock-mounted preamplifier provided with continuous gain control, shaped, and sent to a UCRL model-1000 scaler which was provided with a discriminator. The medium-sized and large-sized signals were amplified to saturation, providing a certain amount of pulse-height selection stability. The proportional nature of the ionization chamber for small signals and the pulse-height requirement used eliminated any possible background from cosmic rays and β and γ activity. The background was always less than 1%, and residual errors from the subtraction were negligible. The correction for fluctuations in the Bevatron beam amplitude was made in the same manner as it was for the β counting. No corrections were needed for scattering in the walls and supporting tray, for air or window absorption, or for dead time (because the recovery time of an ionization chamber is much faster than that of a Geiger counter).

Two corrections remain. The geometrical efficiency of the chamber is exactly 50%, but some alphas traveling slightly downward from the horizontal and slightly below the surface of the foil may be scattered up into the chamber, raising the efficiency to perhaps 51% or 52%. Also the effective thickness of the foil is unknown. Because the α particles leaving the surface of the foil will now produce a continuous spectrum of pulse heights, the exact value of the effective thickness will depend on the gain and pulse-height discrimination of the amplifier and scaler. Therefore, they must be very precisely controlled. If this is done, Au foils may be used as a relative monitor when target materials or energies are changed, something that cannot be done with the pion telescope. The gain and pulse-height discrimination were controlled by using a thick (0.001-in.) standard foil that provided a continuous spectrum of alphas rather than the usual thin standard used in α counting. The standard was counted every 10 or 15 minutes in each of the two chambers used. If the count varied by more than 1% the gain or pulse-height discrimination was adjusted to bring it back to the standard value and another count was taken. If the variation was less than 1%, the measured deviation was used to correct the preceding and following runs with the Au foil. After this had been done, the counting rates of the two Au foils that were counted simultaneously in different chambers always agreed to within the counting statistics of about 1%.

After changing foils, methane was run into the chamber at a high rate to flush out the oxygen, which traps the free electrons produced in the ionization and then causes reduced pulse height. Counting was not started until a monitoring oscilloscope showed the signal had reached full height.

The absolute calibration to determine the effective thickness of the Au foil will require another Bevatron run of several hours. A foil sandwich consisting of a 0.001-in. Al guard foil, 0.003-in. Al foil, 0.001-in. Al guard foil, 0.001-in. Au foil, 0.001-in. Al guard foil, 0.001-in. Au foil, and a 0.001-in. Al guard foil will be plunged in the Bevatron beam. The Al will now not have any error from secondary

target neutrons, and the Na^{24} β activity and its fast daughter γ activity will be counted in a β-γ coincidence counter in which the true rate is

$$\frac{(\beta \text{ counting rate})\ (\gamma \text{ counting rate})}{(\beta\text{-}\gamma \text{ coincidence counting rate})}$$

$$= \frac{(\beta \text{ efficiency})\ (\text{true rate})\ (\gamma \text{ efficiency})\ (\text{true rate})}{(\beta \text{ efficiency})\ (\gamma \text{ efficiency})\ (\text{true rate})} .$$

Thus there will be no corrections for scattering, attenuation or other factors entering into the all-over efficiency. The results from this will then be used to calibrate the α counting. This calibration together with a precise value for the surface area of the standard foil used (which has been determined with a traveling stage microscope to within 0.1%) will allow use of this method with other counters and standard foils without a recalibration.

In order to achieve the 1% accuracy of which this method is capable, it is necessary to line up the edges of the foil and target the beam strikes first to within about 20 microns because of the much greater intensity of the beam on this edge. (Ten percent of the beam strikes the end 400 microns of the target.)

VII. EVALUATION OF DATA

A. Background and Corrected Data

The basic data, the γ-telescope counts divided by the pion-monitor counts as a function of γ-telescope position, must be corrected for a number of background effects.

The main sources of γ-telescope counts with the converter in and the collimation open, and viewing the region near the target are given in Table II.

Table II

Estimated counting rate[a]	Source of count
1a. 10^{-2} to 10^{-4}	$K^0 \rightarrow$ neutral pions $\rightarrow$ gamma rays; γ converts in the converter (rate is a function of telescope position).
1b. 10^{-3} to 10^{-5}	Same, but γ converts in the back of A or the front of S1 (about 1/20 radiation length is available).
2a. 10^{-3} to 10^{-5}	Target $\pi^0 \rightarrow \gamma$ rays; $\gamma \rightarrow e^+ + e^-$ near the face of collimator 1 (lowest collimator), $e^{\pm} \rightarrow \gamma$ near the face of highest collimator, γ converts in the converter (estimated from below-threshold data).
2b. 10^{-4} to 10^{-6}	Same, but last γ converts in A or S1.
3a. 10^{-4}	A neutron penetrates collimator 1 and some upper collimators and makes a charged particle in the converter.
3b. 10^{-4}	Same, but makes the charged particle in A or S1 (about as much collision length is available in A or S1 as in the Pb converter).
4a. 10^{-5}	A neutron passes through the hole in collimator 1 and some upper collimators, and makes a charged particle in the converter.

Table II (continued)

	Estimated counting rate[a]	Source of count
4b.	10^{-5}	A neutron passes through the hole in collimator 1 and some upper collimators, and makes a charged particle in A or S1 (estimated from 3, the hole area is about 0.02 of the collimator area, collimator is only about -1/2 collision-length thick).
5a.	10^{-5}	A neutron or $\pi^{\pm}$ penetrates collimator 1, producing $\pi^0 \rightarrow \gamma$ in collimator 2 or above; the γ converts in the converter. (Mostly neutrons penetrate the collimator. Two inches of Pb is observed to cut the charged particle flux by a factor of about 10.)
5b.	10^{-6}	Same, but the γ converts in A or S1. (Number of counts here are estimated to be smaller than those for 4 because the converter-in-converter-out ratio approaches $\sim$ 1 with collimator 1 blocked).
6a.	10^{-6}	A neutron or $\pi^{\pm}$ passes through the hole in collimator 1, scatters in collimator 2 or above to reach a viewed area of an upper collimator, producing $\pi^0 \rightarrow \gamma$; γ converts in the converter. (Neutrons are the main source of this effect.)
6b.	10^{-7}	Same, but the γ converts in A, S1 (6 is smaller than 5 for same reason that 4 is smaller than 3).
7a.	10^{-6}	Neutron or $\pi^{\pm}$ produces a $\pi^0 \rightarrow \gamma$ near face of collimator 1, γ "scatters" ($\gamma \rightarrow e^{\pm} \rightarrow \gamma$) from faces of upper collimators, converts in the converter.
7b.	10^{-7}	Same, but the γ converts in A, S1.

[a] On-target rate $\equiv$ 1

When the counting rate is taken with the converter out and subtracted from the converter-in data, all the "b" classifications above are eliminated. This removes the rather large contribution from 3b and is also necessary because the telescope is calibrated correctly only for those γ rays converting in the converter.

When the hole in collimator 1 is closed, the following things contribute to the converter-in–converter-out difference:

3a.		Same as before
4a.		About half the contribution with collimator open
5a.		Same as before
6a.		About half the contribution with collimator open
1a, 2a, 7a		Essentially zero because a γ will not penetrate 10 radiation lengths of lead with a reasonable probability.

An additional source of background now enters:

8a.	$< 10^{-4}$	A neutron or $\pi^{\pm}$ makes $\pi^0 \rightarrow \gamma$ rays near top of the block closing collimator 1, the γ converts in the converter. This source is estimated to be less than 10^{-4} because the 10^{-4} counting rate observed with the channel closed has a converter-in–converter-out ratio of near 1.

Subtracting the channel-closed data from the channel-open data leaves the following sources of counts:

1a.	10^{-2} to 10^{-4}	K^0 γ rays
2a.	10^{-3} to 10^{-5}	Slit-scattered γ rays from target (10^{-3} corresponds to 10^{-2} of 1a, 10^{-5} to 10^{-4} of 1a).
4a.	10^{-5}	A neutron through the hole produces a charged particle in the converter.
6a.	10^{-6}	A neutron through hole produces a γ in a viewed region.

7a.	10^{-6}	A γ produced by N or $\pi^{\pm}$ in face of collimator 1 scatters its way up.
8a.	$\approx 10^{-5}$	A γ produced by N or $\pi^{\pm}$ in the top of the block.

A similar four-item subtraction taken below associated-production threshold gives mainly 2a with contributions similar to 4a, 6a, 7a, and 8a but reduced in intensity. The energy of most of the γ rays in 2a should not be too much lower than those produced at 6 Bev because much of the additional energy goes into multiple production and the γ energy is Doppler shifted down by a greater amount because of the higher center of momentum velocity. The shape of the counting rate curve as a function of the γ-telescope position should change even less. This was confirmed by an earlier run in which the upstream slope was measured at 3 Bev (below the energy at which K mesons can go upstream). The below-threshold curve, normalized to the same on-target intensity as the above-threshold data, is then subtracted from it to produce the final data for analysis:

$$\text{(Final counting rate)} = \left\{\begin{matrix}\text{above threshold}\\ \text{converter in}\\ \text{channel open}\end{matrix}\right\} - \left\{\begin{matrix}\text{above threshold}\\ \text{converter out}\\ \text{channel open}\end{matrix}\right\}$$

$$- \left\{\begin{matrix}\text{above threshold}\\ \text{converter in}\\ \text{channel closed}\end{matrix}\right\} + \left\{\begin{matrix}\text{above threshold}\\ \text{converter out}\\ \text{channel closed}\end{matrix}\right\}$$

$$- \quad \text{(same four terms below threshold).}$$

Statistical fluctuation, magnified by the many subtractions required, is the main source of error. Further errors, smaller but of comparable magnitude, come from:

(a) Fluctuations in the amount of beam striking the tangent-tank walls and seen by the monitor but not by the γ telescope.

(b) Inexact subtraction of second-order neutron effects (4a and 8a).

(c) Possible differences in the 1- and 6-Bev shapes of the intensity vs. position curves for target γ-rays.

Accidental counts were negligible at the beam intensities used.

An attempt was made to measure the off-target counting rate of γ rays that were scattered by the slits into the counter, relative to the on-target γ counting rate. At energies below the threshold for associated production where such a measurement must be made, the Bevatron beam did not prove stable enough to permit sufficiently long runs. The result for the off-target counting rate below threshold after converter-in–converter-out and channel-open–channel-closed subtractions were made was negative, with statistics easily overlapping zero. Therefore, the correction was made by using data taken previously under more stable conditions with a similar but not identical slit system. The estimated uncertainty in this subtraction is small compared with the statistical error of the final value.

The counting rate is plotted in Fig. 8 as a function of the angle about the vertical axis of the counter and collimation setting. The ordinate of the data taken with the 1-in. radial setting is the counting rate relative to an on-target counting rate. The values of the data taken with the 2-in. setting are multiplied by a factor of:

$$\frac{\text{included angle} \times \text{radial length} \times \text{solid angle (for 1-in. slits)}}{\text{included angle} \times \text{radial length} \times \text{solid angle (for 2-in. slits)}}$$

$$= \frac{30^\circ}{22\text{-}1/2^\circ} \times \frac{1/2 \text{ in.}}{1 \text{ in.}} \times \frac{1}{3} = \frac{1}{4.5} .$$

Because particles with projected decay distances long compared with 2-in. would give 4.5 times as many counts as the 2-in. setting as the 1-in. setting, dividing by 4.5 makes the actual decay distances more apparent.

Only statistical errors are shown.

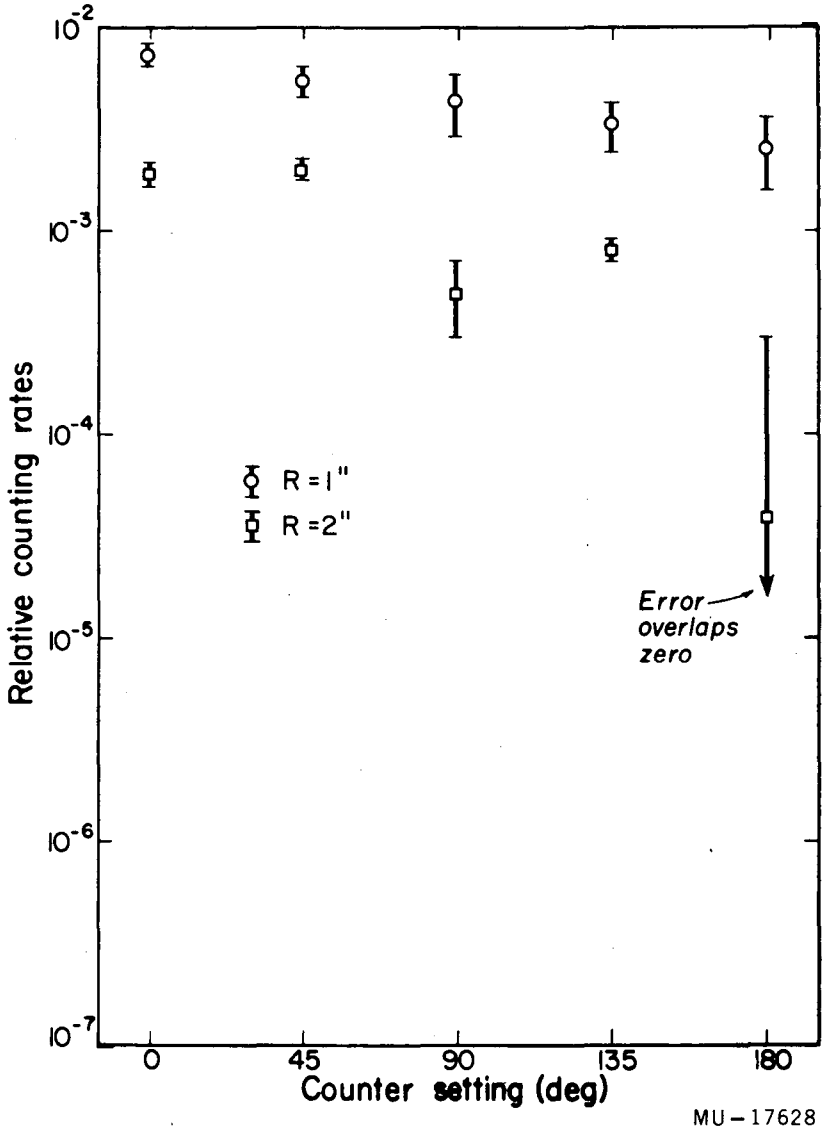

Fig. 8. Gamma counting rate at 6 Bev corrected for background. On-target rate ≡ 1.0.

B. Calculated Values

In order to fit the experimental data, a general model of the production and decay of particles with γ decay modes is assumed. The predicted number of γ rays to be detected per incident proton is calculated and compared with the experimental data. The parameters of the model are varied in order to give a best fit and to see what range is consistent with the data.

As an example, for the most important source of observed γ rays, the K^0, the production can occur in such ways as:

$p + \text{nucleon} \rightarrow K^0 + \Sigma + \text{nucleon}$

$p + \text{nucleon} \rightarrow K^0 + \Lambda + \text{nucleon}$

$p + \text{nucleon} \rightarrow K^0 + \bar{K}^0 + \text{nucleon} + p$

$p + \text{nucleon} \rightarrow K^0 + \Sigma + \text{nucleon} + \pi$

$p + \text{nucleon} \rightarrow K^0 + \Lambda + \text{nucleon} + \pi$

$p + \text{nucleon} \rightarrow K^0 + \bar{K}^0 + \text{nucleon} + \text{nucleon} + \pi$

In addition, such second-order reactions as the following will contribute:

$p + \text{nucleon} \rightarrow K^{\pm} + \text{similar reaction products,}$

$K^+ + \text{neutron (in the same nucleus)} \rightarrow K^0 + p$

$K^- + p \rightarrow \bar{K}^0 + \text{neutron}$

$p + \text{nucleon} \rightarrow \pi + \text{other reaction products,}$

$\pi + \text{nucleon (in same nucleus)} \rightarrow K^0 + Y$

The K^0 mesons leave the surface of the nucleus with some resultant distribution in energy and polar angle, θ. They then decay, some in view of the counter. Some of these send a γ from the decay-produced π^0 into the solid angle of the counter with sufficient energy to count.

An exact calculation would then involve an integration over all parameters representing the chain of possible events inside the nucleus, the distance traveled before decay, the direction of the decay π^0, and the direction of its decay γ. This would have to be repeated for γ rays coming from Σ, Λ, and $K^{\pm}$ decay.

The point to be made here is that this would be unnecessarily complicated (as well as being impossible). A natural breaking point occurs in this problem--the surface of the nucleus. A distribution in energy and angle of particles leaving the surface is assumed and varied to fit the data. Any detailed study of what happens inside the nucleus would need to predict this calculated distribution at the surface.

If the production occurred through the three-body final state K + Y + nucleon with the K escaping from the nucleus with no further interaction, the number of γ rays observed would be proportional to an integration over

$$b\, G(N)\, F(N, E_{Uc})\, |M(N, E_{Uc}, \theta_{Uc})|^2\, P(\text{position}, N, E_{Uc}, \theta_{Uc}, \phi).$$

Here b is the branching ratio for γ decay; G(N) is the number of initial states as a function of c.m. energy N(not a delta function, because of spread in beam energy and Fermi momentum of nucleon); $F(N, E_{Uc})$ is the three-body phase-space factor; $|M(N, E_{Uc}, \theta_{Uc})|^2$ is the production-matrix element squared; $P(\text{position}, N, E_{Uc}, \theta_{Uc}, \phi)$ is the probability of detecting the decay γ as a function of counter position, N, and energy and angle of the unstable particle; and $F \times |M|^2$ is equivalent to the phenomenological distribution as the particle leaves the surface of the nucleus. In the calculations described in detail in the Appendix, G and P are effectively factored out. The three-body phase space factor F is also included in these calculations, because, even in a phenomenological approach $|M|^2$ is more interesting than the product $F \times |M|^2$.

Once the relative value of $|M|^2$ is determined, the absolute cross section for an unstable particle (U) can be calculated from:

$$\frac{\sigma N' \rho t}{A} = \frac{\text{No. U}}{\text{proton}} = \frac{(\text{No. } \gamma/\text{proton})}{(\text{No. } \gamma/\text{U decay})(b)}$$

$$= \frac{(\text{No. } \gamma \text{ produced})}{(\text{No. } \gamma \text{ observed})} \quad \frac{(\text{No. } \gamma \text{ observed/proton})}{(\text{No. } \gamma/\text{U decay})\ (b)} .$$

Rearranging terms and substituting a more specific expression for γ produced/γ observed, we have

$$\sigma = \frac{A}{N' \rho t} \quad \frac{(\text{No. } \gamma \text{ observed/proton})}{(\text{No. } \gamma/\text{U decay})} \quad (b)$$

$$\times \frac{\int_N dN \int_{E_U} dE_U \int_{\theta_U} d\theta_U \int_{\phi_U} d\phi_U \int_{E\gamma} dE\gamma \; G(N) F(N, E_U) \left| M(N, E_U, \theta_U) \right|^2}{\int_N dN \int_{E_U} dE_U \int_{\theta_U} d\theta_U \int_{\phi_U} d\phi_U \int_{E\gamma} dE\gamma \; G(N) F(N, E_U) \left| M \right|^2 P(\text{geom}, N, E_U, \theta_U, \phi_U}$$

where σ is the total cross section, N' is the Avogadro's number, ρ is the target density, t is the target thickness (small compared with an interaction length), and A is the target atomic number. The last factor is the reciprocal of the average detection efficiency of the decay gammas.

C. Comparison of Data with Calculated Values

The calculated values of the predicted relative counting rates are plotted in Figs. 9 to 12 for various assumptions about the angular and momentum dependence of the production matrix element. The ordinate for the 1-in. curves is the effective counting probability (the number of counts per K particle leaving the nucleus) at a given position. The ordinate for the 2-in. curves is the predicted probability divided by 4.5 to make the actual decay distance more apparent and to agree with the plot of the experimental data. The abscissa is the angular position of counter and collimation assembly.

The knowledge of three things will help in interpreting the data and calculations. These are:

(a) Because of their relatively low velocities in the center-of-momentum system, hyperons cannot directly cause counts with the counter set at 180°, 135°, and 90°, and can give only a very limited number at the 45° setting. Even at 0°, their lower Q values and velocities make it difficult for them to send a high-energy gamma to the detector. Thus, the data primarily provides information about the K production and decay parameters. The longer mean life of the K^{+} and the fact that it produces only 2 γ rays depresses its calculated counting probability by a factor of about 15 below that of the K^{0} at the 1-in. setting.

(b) With the counter set at 0° or 45°, K particles starting forward in the center-of-momentum system are less likely to produce counts than those starting backwards and being transformed forward by the center-of-momentum velocity. The factor between their counting probabilities is generally larger than 10^{2}. This is because the ones that started forward are traveling fast enough to Doppler shift the energy of γ rays coming out vertically to energies at which the counter has a zero or nearly zero efficiency. Thus the data provide information on the angular distribution in the backwards hemisphere. Complications due to a possible forward-backward asymmetry are absent. Counting rates at the 0° and 45° settings are most sensitive to the values of the angular-distribution function from 90° to about 160° in the center of momentum; counting rates at the 180° setting depend almost entirely on the values of the angular-distribution function close to 180°.

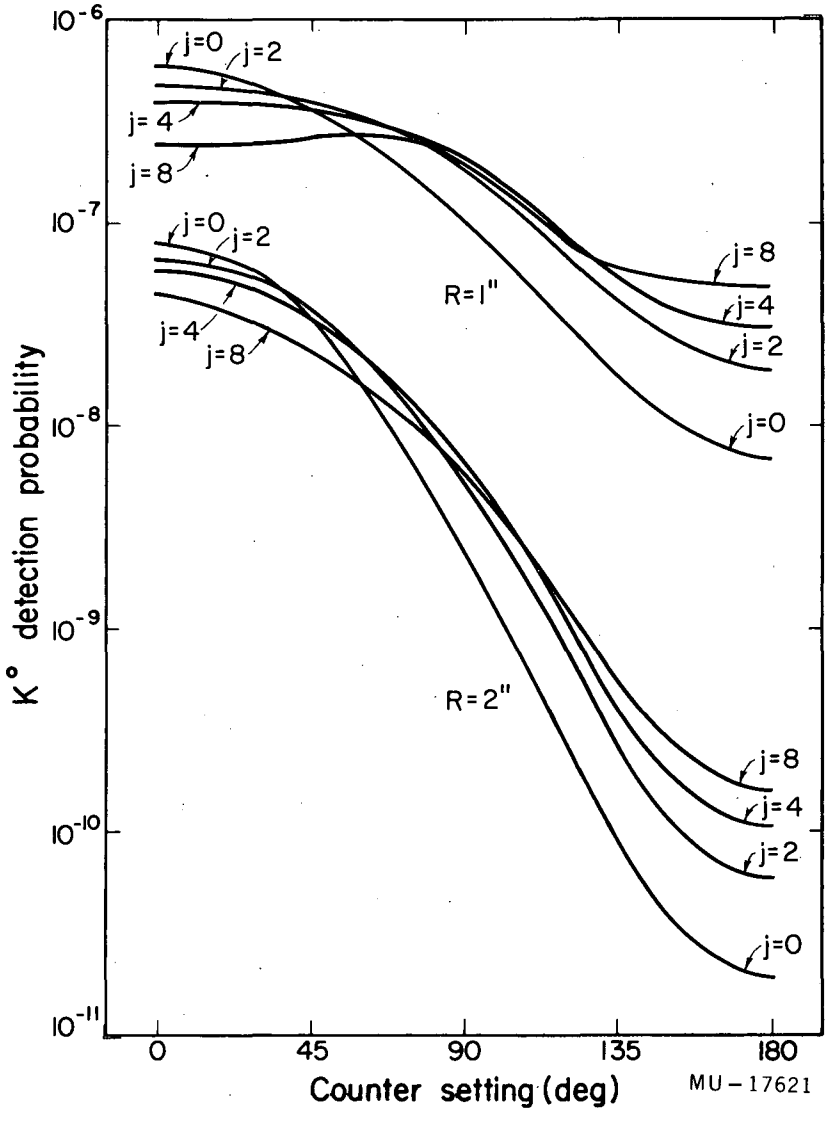

Fig. 9a. K^0 detection probability vs. counter setting. $|M|^2 \sim \cos^0\theta_{Kc}(P^2_{Kc})^j$.

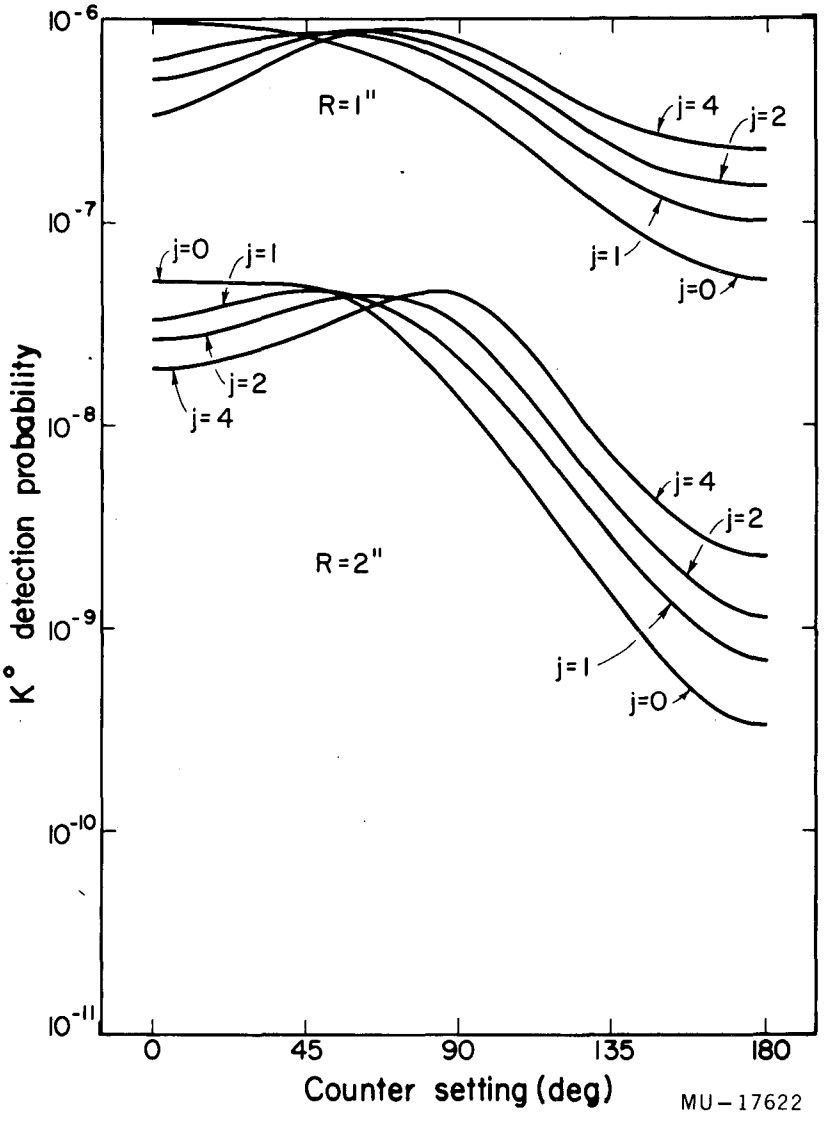

Fig. 9b. K^0 detection probability vs. counter setting. $|M|^2 \sim \cos^8 \theta_{Kc} (P^2_{Kc})^j$.

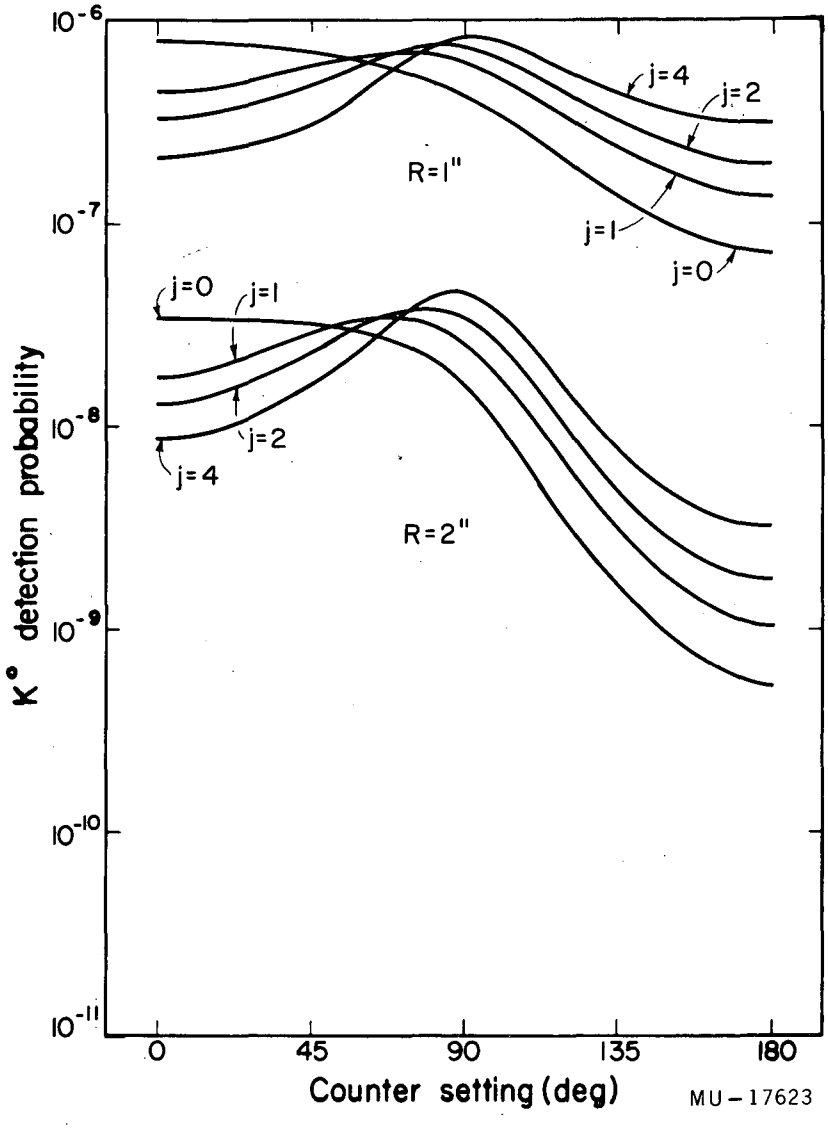

Fig. 9c. K^0 detection probability vs. counter setting. $|M|^2 \sim \cos^{12}\theta_{Kc}(P^2_{Kc})^j$.

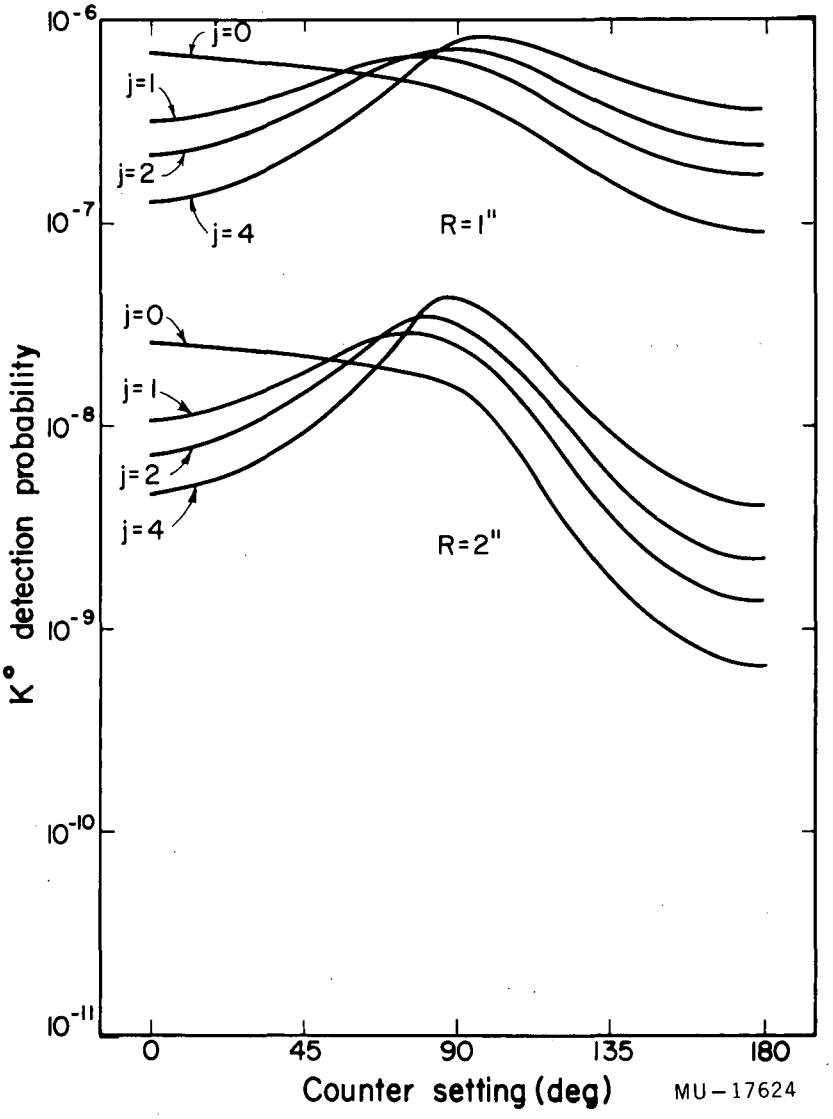

Fig. 9d. K^0 detection probability vs. counter setting. $|M|^2 \sim \cos^{16}\theta_{Kc}(P^2_{Kc})^j$.

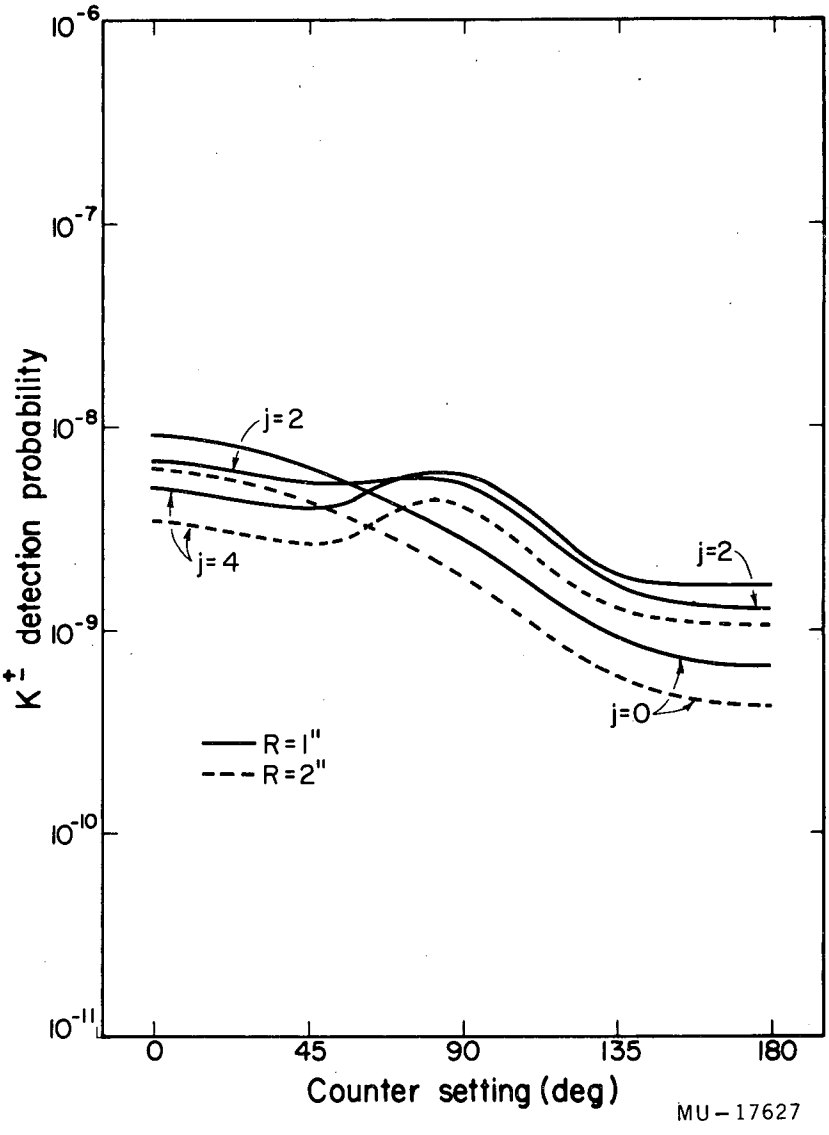

Fig. 10a. K^+ detection probability vs. counter setting. $|M|^2 \sim \cos^0 \theta_{Kc} (P^2_{Kc})^j$ (Only two curves for R = 2 in. are shown as samples. For all K^+ curves, values at R = 2 in. are from 0.58 to 0.68 of those at R = 1 in.)

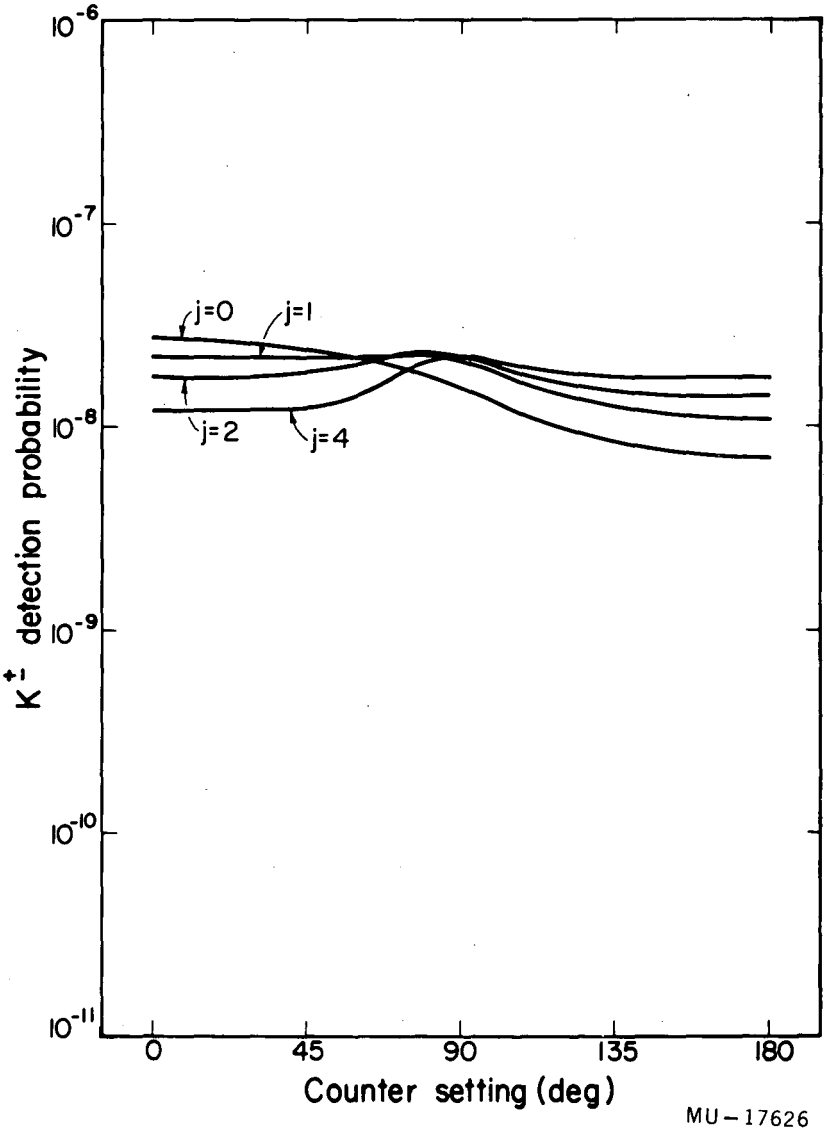

Fig. 10b. K^+ detection probability vs. counter setting. $|M|^2 \sim \cos^8 \theta_{Kc} (P^2_{Kc})^j$ (All values at R = 2 in. are from 0.58 to 0.68 of those at R = 1 in.)

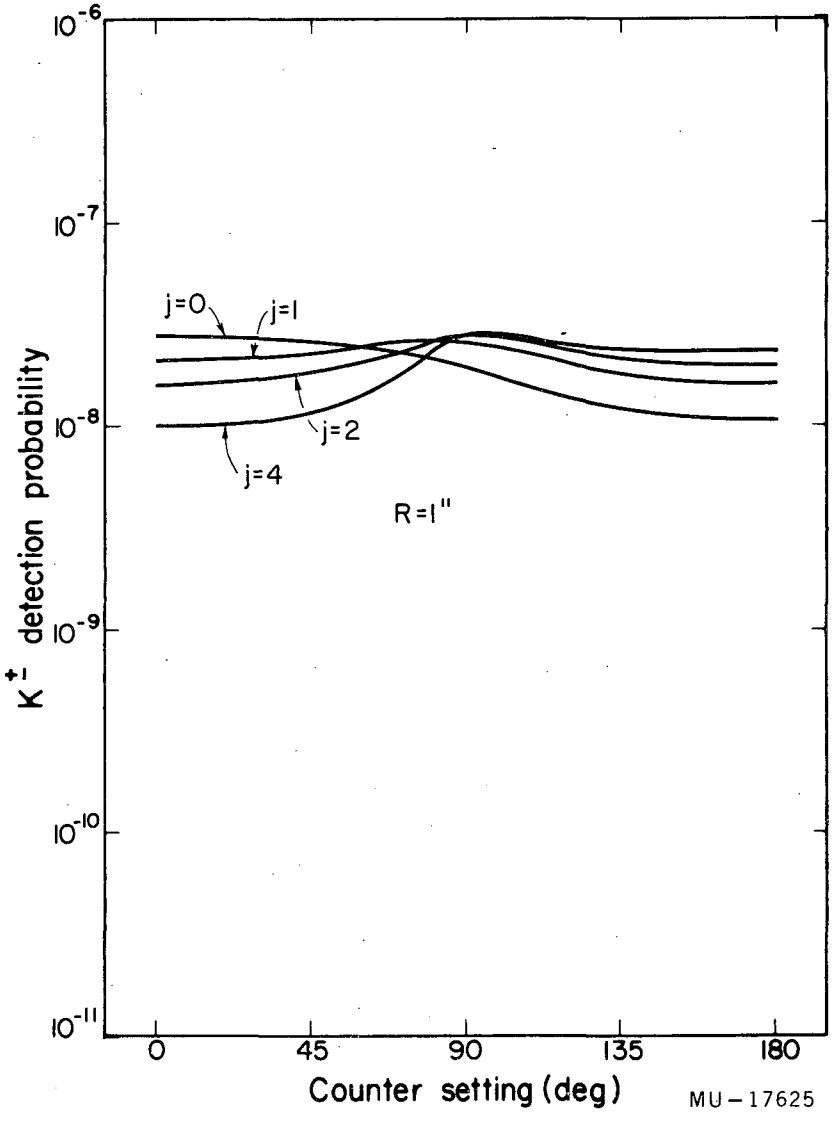

Fig. 10c. K^+ detection probability vs. counter setting. $|M|^2 \sim \cos^{12}\theta_{Kc}(P^2_{Kc})^j$ (All values at R = 2 in. are from 0.58 to 0.68 of those at R = 1 in.)

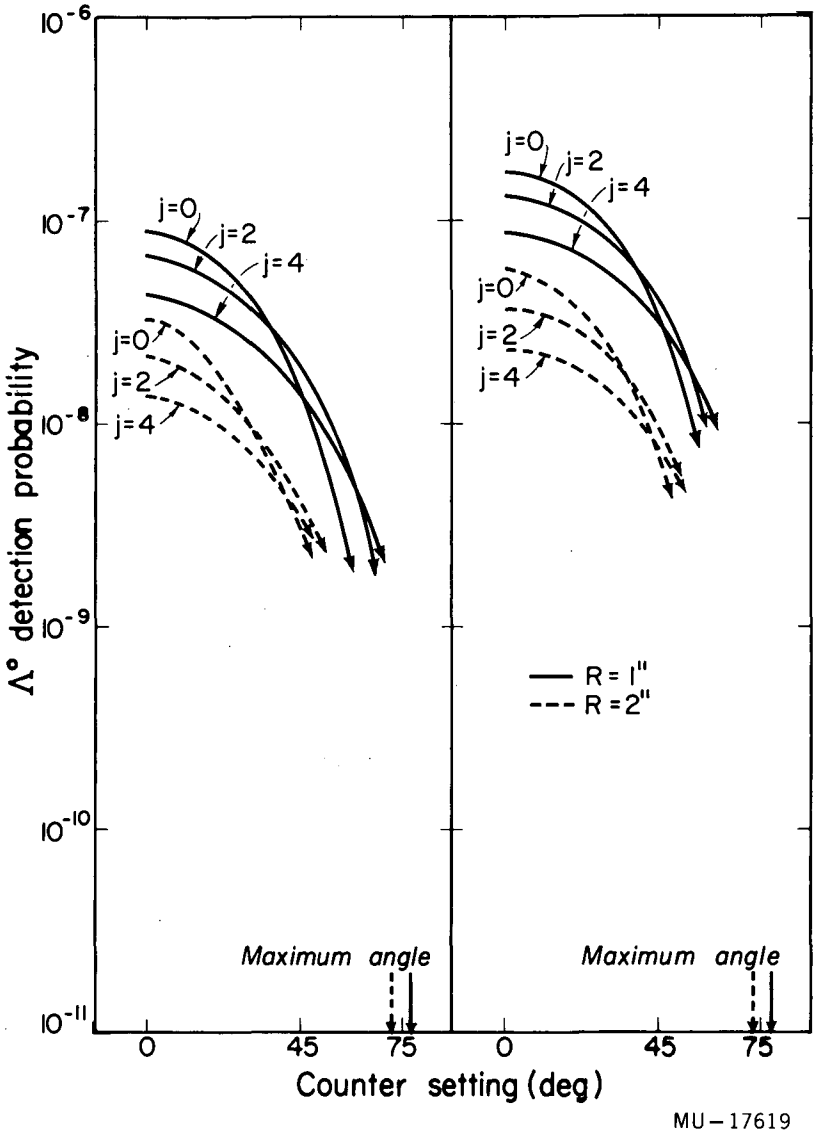

Fig. 11a. Λ^0 detection probability vs. counter setting.
(left) $|M|^2 \sim \cos^0 \theta_{\Lambda c} (P^2_{\Lambda c})^j$
(right) $|M|^2 \sim \cos^2 \theta_{\Lambda c} (P^2_{\Lambda c})^j$. Dotted and solid arrows indicate maximum angles at which Λ^0 decays can be observed at R = 2 in. and R = 1 in. respectively.

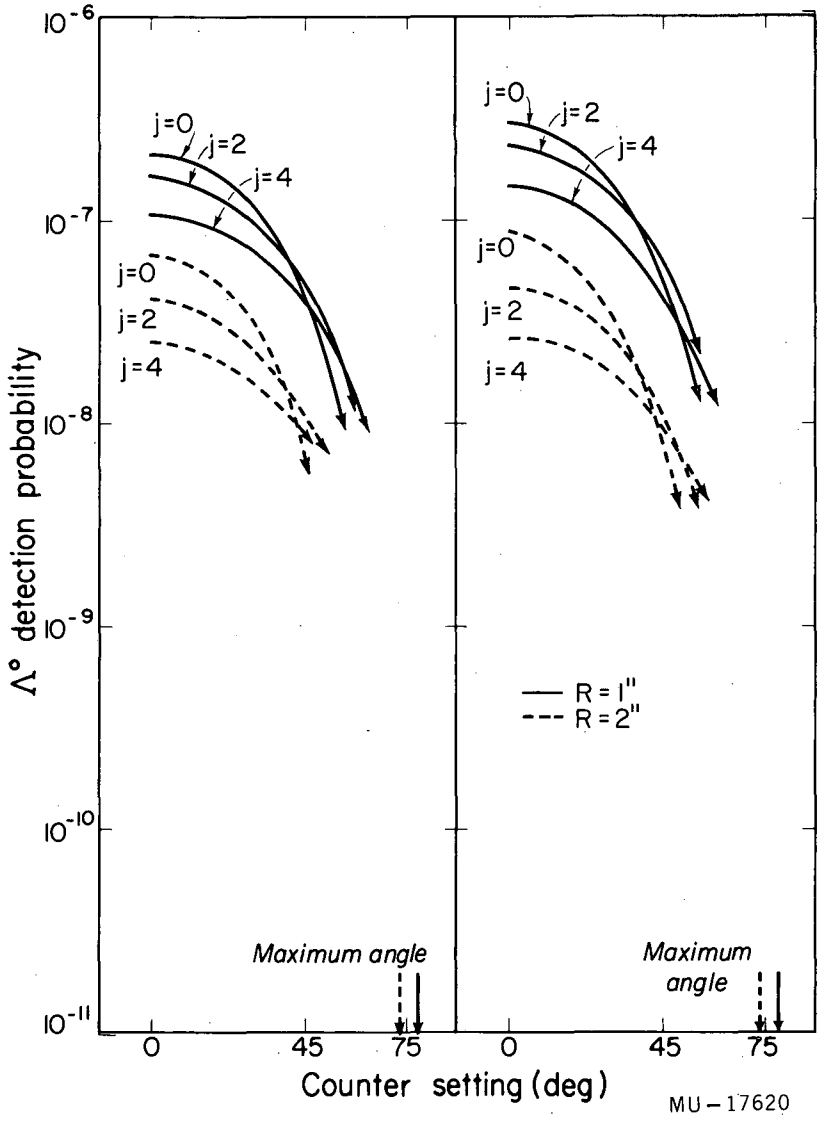

Fig. 11b. Λ^0 detection probability vs. counter setting.
(left) $|M|^2 \sim \cos^4 \theta_{\Lambda c} (P^2_{\Lambda c})^j$
(right) $|M|^2 \sim \cos^{16} \theta_{\Lambda c} (P^2_{\Lambda c})^j$. Dotted and solid arrows indicate maximum angles at which Λ^0 decays can be observed at R = 2 in. and R = 1 in. respectively.

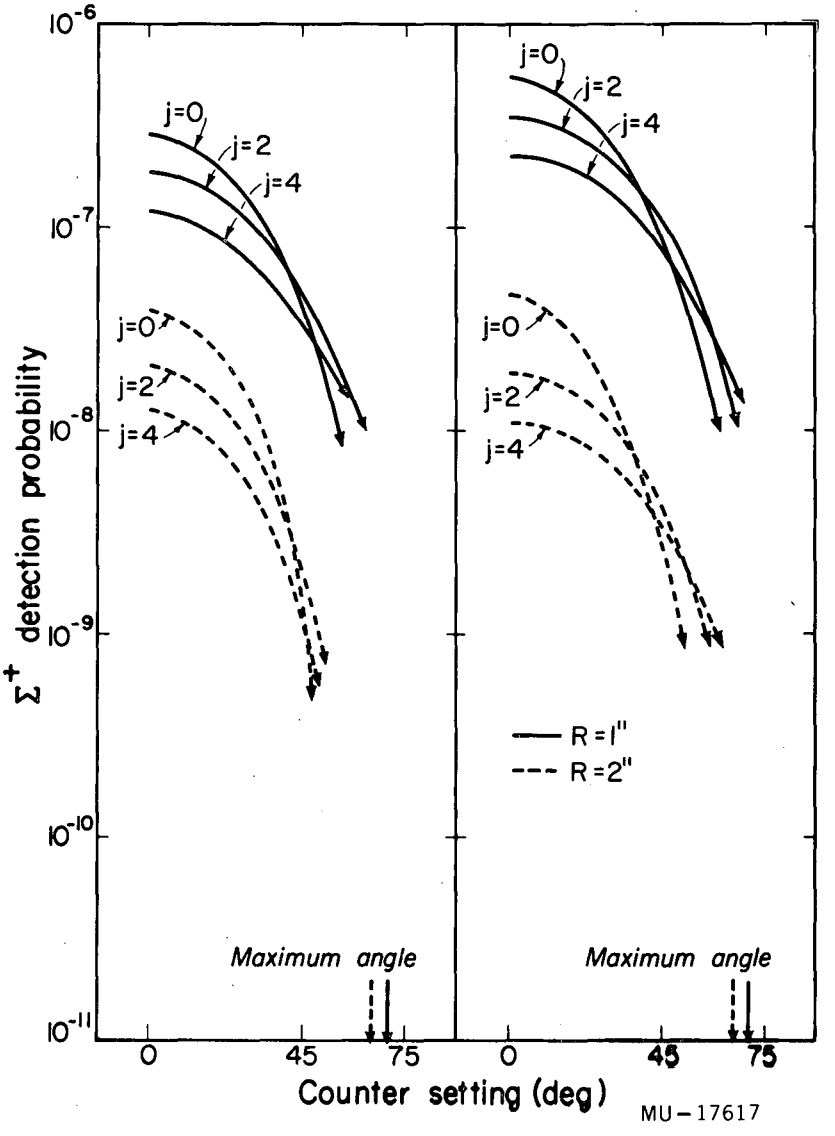

Fig. 12a. Σ^+ detection probability vs. counter setting.
(left) $|M|^2 \sim \cos^0 \theta_{\Sigma c} (P^2_{\Sigma c})^j$
(right) $|M|^2 \sim \cos^4 \theta_{\Sigma c} (P^2_{\Sigma c})^j$. Dotted and solid arrows indicate maximum angles at which Σ^+ decays can be observed at R = 2 in. and R = 1 in. respectively.

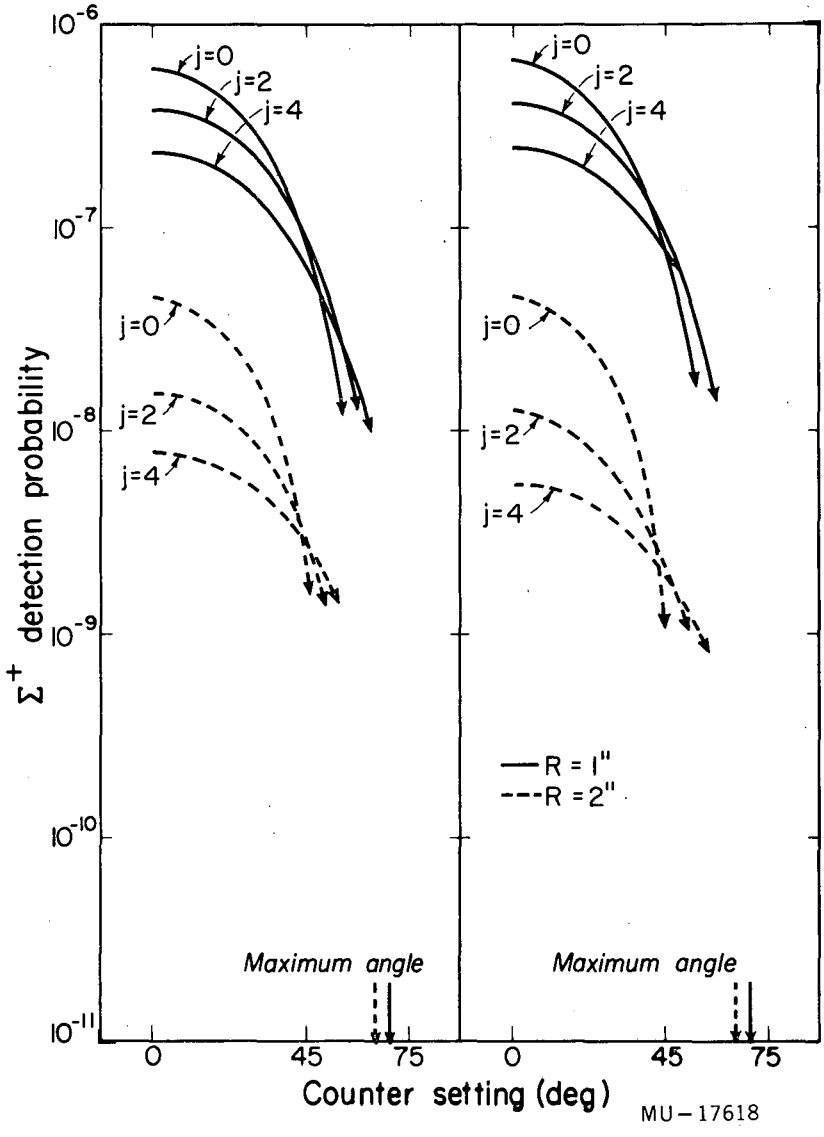

Fig. 12b. Σ^+ detection probability vs. counter setting. (left) $|M|^2 \sim \cos^8 \theta_{\Sigma c} (P^2_{\Sigma c})^j$ (right) $|M|^2 \sim \cos^{16} \theta_{\Sigma c} (P^2_{\Sigma c})^j$. Dotted and solid arrows indicate maximum angles at which Σ^+ decays can be observed at R = 2 in. and R = 1 in. respectively.

(c) A high power of momentum dependence in the matrix element will cause a higher counting rate at counter settings of 135° and 180° and a lower rate at 0° and 45°. The reason for the increased upstream counting rates is clear: an increased power of momentum dependence weights more heavily the higher-momentum K's which can fight their way upstream most easily. The reason for the decreased rate downstream is not quite so obvious. Almost all downstream counts come from low-and medium-energy particles that head upstream in the center-of-momentum system but come out downstream in the laboratory system. A dependence on a high power of the momentum puts very little weight on these particles.

From a comparison of the calculated curves shown in Figs. 9 to 12 and the experimental values shown in Fig. 8 it is clear that, for $k \leq 16$, no single value of j and k in the matrix element will give satisfactory agreement with the experimental data. The best is $j = 0$, $k = 16$, and that misses the points by an average of over one standard deviation. A close fit would require $j = 0$, $k \cong 30$. Since it seemed unlikely that such a high angular-momentum state would occur alone, no exact calculations were carried out for $k > 16$. Instead combinations of two angular and momentum dependences were tried. From Figs. 9 to 12 it is clear that at least one of these must have $j = 0$. Best fits for $j = 0$, $k = 0$ and $j = 1$, $k = 12$, and 16; $j = 2$, $k = 8$, 12, and 16; $j = 4$, $k = 8$, 12, and 16; $j = 8$, $k = 8$, 12, and 16 are shown in Table III. For comparison, the values for $j = 0$, $k = 0$ have also been included.

The K^0 counting rate to be fitted was calculated by using the ratio between the counting rates at r = 1-in. and r = 2-in. for $\alpha = 45^{\circ}$, 90°, 135°, and 180°, and the ratio between the counting probabilities for the K^0 and $K^{\pm}$ at these positions to estimate the fraction of the counts due to K^0 decay at 1-in. ($\sim 75\%$). The errors shown now include both statistical errors and an estimate of the somewhat smaller error due to the uncertainty in the subtraction of the $K^{\pm}$ counts. The conclusions reached in the following section are quite insensitive to the magnitude of this correction and remain substantially the same even with no subtraction of $K^{\pm}$ counts.

Table III

K^0 matrix element of form $1 + a_{j\,k}(P^2_{Kc})^j \cos^k \theta_{Kc}$ †

		Relative amounts		Average error (in standard deviations)	Calculated relative counting rates (normalized to observed rate) r = 1-in.				
		Isotropic	Peaked						
j	k	a'*	a''*		$\alpha = 0^o$	$\alpha = 45^o$	$\alpha = 90^o$	$\alpha = 135^o$	$\alpha = 180^o$
-	-	1.0	0	1.52	59	36	10	1.7	0.7
2	8	0	0.59	1.02	28	45	40	14	8.3
4	8	0.22	0.48	0.85	29	41	40	16	11
8	8	0.34	0.47	0.69	27	39	41	19	16
1	12	0.034	0.64	0.91	30	38	40	14	8.6
2	12	0.29	0.50	0.91	33	34	39	30	9.8
4	12	0.41	0.48	0.62	34	30	44	21	15
8	12	0.65	0.38	0.43	42	29	39	22	18
1	16	0.22	0.63	0.79	33	37	42	17	10.5
2	16	0.14	0.66	0.80	29	35	42	18	10.9
4	16	0.58	0.43	0.46	40	30	40	23	16
8	16	0.68	0.38	0.28	42	28	36	26	19
		Experimental K^0 counting rates			40 ± 20	30 ± 15	29 ± 15	29 ± 13	22 ± 10

*(isotropic-component detection efficiency × a') + (peaked-component detection efficiency × a'') = $\frac{(\gamma \text{ counts, } r = 1 \text{ in.}) \times 10^{-4}}{\gamma \text{ counts, } r = 0 \text{ in. (on target)}}$.

† K_1^0 mean life is assumed to be 0.95×10^{-10} sec.

Although $K^{\pm}$ decays were responsible for over 80% of the counts at r = 2-in. and $\alpha = 45^{\circ}$, 90°, 135° and 180°, it is not possible to deduce the production matrix element from this data because of the insensitivity of the counting probability to changes in the matrix element (Fig. 10). It is also not possible to say anything about the detection of counts from Λ and Σ hyperons except that the data is consistent with their existence at 0° providing they are responsible for less than half of the counting rate there. At 45° they could not be an important part of the counting rate.

No subtraction for Λ and Σ counts was made at 0°. A subtraction would decrease the counts apparently due to K^0's at 0° and increase even further the peaking required of the K^0 matrix element. Thus again the conclusions concerning strong angular dependence of the K^0 production are not weakened.

Several representative cases are plotted in Figs. 13 and 14.

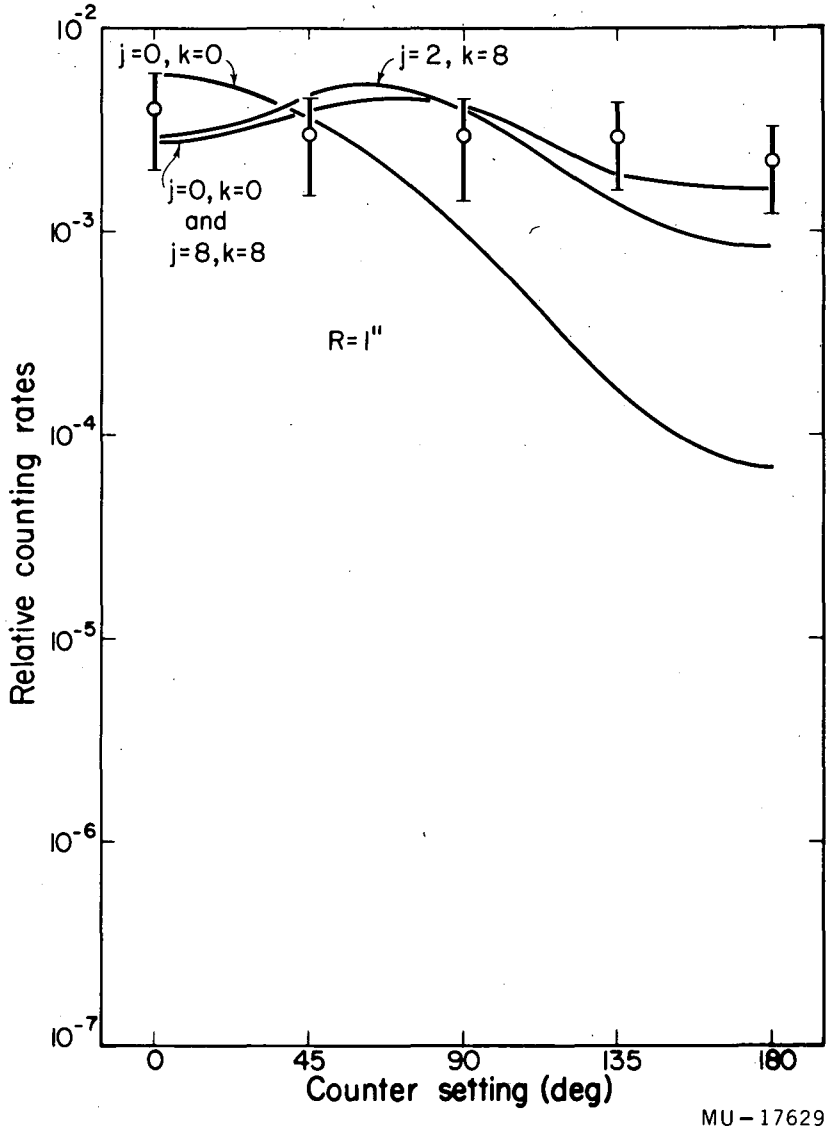

Fig. 13. Calculated relative counting rates and K^0 counting rate vs. counter setting. (K^0 rate = experimental rate - calculated K^+ rate.)

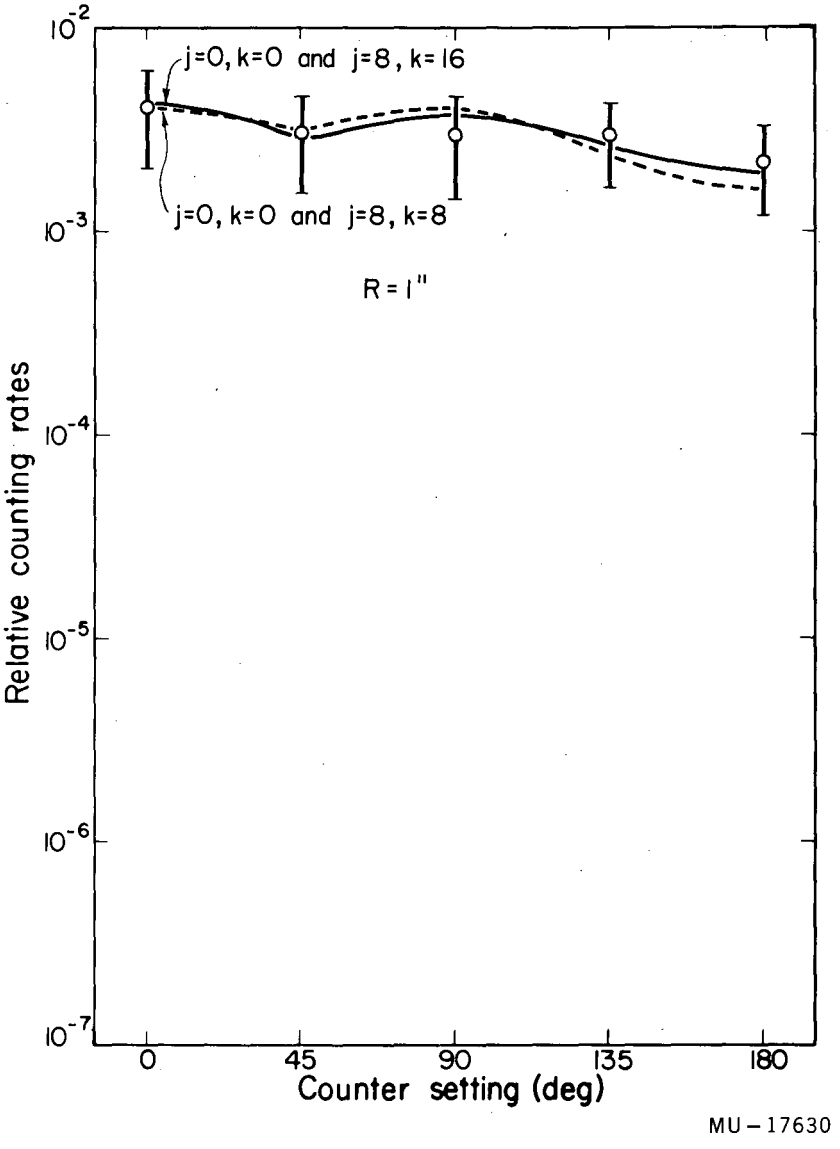

Fig. 14. Calculated relative counting rates and K^0 counting rate vs. counter setting. (K^0 rate = experimental rate - calculated K^+ rate.)

VIII. CONCLUSIONS

(a) Of the known decay schemes, only $K^0 \rightarrow \pi^0 + \pi^0$, $\pi^0 \rightarrow \gamma + \gamma$ can be responsible for most of the γ rays observed.

(b) The data cannot be fit by a matrix element of the form $|P_{Kc}{}^2|^j \cos^k \theta_{Kc}$ for $k \leq 16$ and any value of j. A matrix element with $j = 0$, $k \cong 30$ would probably fit, but the counting probability as a function of position for such a matrix element was not computed because it seems unlikely that such a term would exist alone.

(c) A combination of two terms of the form $|P^2_{Kc}|^o \cos^{k'} \theta_{Kc} + |P^2_{Kc}|^j \cos^k \theta_{Kc}$ can fit the data taken at a radius of 1 in. For $k' = 0$ (making the first term S wave), the best fits occur for $k = 12$, $j \geq 4$; $k = 16$, $j \geq 4$, with the fit improving as j and k increase. Values of k above 16 are not needed for a satisfactory fit, but cannot be excluded by the data. Also, increasing j above about 8 does not materially improve the fit, but also does not worsen it. This is because the strongest weighting is merely being shifted to a value of E_{Kc} only slightly nearer E^{max}_{Kc}.

(d) Too much significance should not be attached to the exact value of j. The form of the momentum dependence in the matrix element, $|P^2_{Kc}|^j$, comes from theoretical considerations that are expected to be valid only for K mesons with low energy in the center-of-momentum system. These K particles have a low counting probability and will not significantly affect the results. The values here obtained for j should simply be considered as requiring that considerably more K mesons be produced at high energy than a three-body statistical factor would indicate.

(e) The decrease in counting rate as the radius increases is too slow to be explained only by a K^0 lifetime of 0.95×10^{-10} seconds. It is however quite consistent at all angles with a composite decay curve due to K^0 and $K^{\pm}$ decays. The ratio of counting rates at 1 and 2 in. indicates that the K^0 produces most of the counts at 1 in., and the $K^{\pm}$ produces most of those at 2 in. The predicted detection efficiency at 2 in. is not a sensitive enough function of the $K^{\pm}$ matrix element to permit a determination of it.

(f) The conclusion that has been drawn in (c) that an important part of the K production is sharply peaked in energy and angle is not weakened by the assumption of a three-body model for the kinematical analysis.

The energy dependence of a composite phase-space factor that includes contributions from processes such as

nucleon + nucleon → nucleon + hyperon + K + several pions

would be weighted toward lower energy K mesons than that for a three-body process. This however would require an even higher value of j in the multiplying factor of $|P_{Kc}^2|^j$ to match the experimental data. Production of K mesons with several associated pions affects only one other thing in the kinematical analysis, the value of E_{Kc}^{max}, and this only slightly.

The production of K^0 mesons through charge exchange of $K^{\pm}$ particles on nucleons or collisions of intermediate pions and nucleons also does not weaken the conclusion about the peaked component of K^0 mesons. What is observed is a peaking, especially in angle, of K^0 mesons leaving the nucleus. The above two production mechanisms can only reduce the observed peaking and thus require that the fundamental reaction

nucleon + nucleon → nucleon + hyperon + K

produce even more sharply peaked K mesons.

Finally, the data could be fit by a more complicated matrix element, such as one in which the angular distribution is a function of K energy or one using many terms with different powers of P_{Kc}^2 and $\cos \theta_{Kc}$. A matrix element with several low powers of $\cos \theta_{Kc}$ could not replace one with one high power, because the ratios of detection probabilities at 180° to those at 0° would be too low for all terms. If low-power terms are to be added, additional high-power terms will also be needed.

Our data, however, which involves contributions from a range of P_{Kc} and θ_{Kc} for each experimental point, does not justify such a detailed treatment and little would be learned from one. Any such matrix element would have to have the same gross features as the

simpler matrix elements for the upstream K mesons which are most likely to be detected--part approximately flat and part very sharply peaked--and could do whatever it wanted elsewhere.

A strong peaking such as we have observed could be explained by a phenomenological stripping model described by Peaslee.[15] The long range interactions $\left(> \frac{\hbar}{m_{Kc}}\right)$ needed to give this peaking have been further developed by Barshay[16] and Schwinger.[17].

In Peaslee's model, one nucleon is considered to be "predissociated" into a virtual K and a virtual Λ or Σ. The hyperon is then "stripped" by an interaction with a pion from the cloud around the other nucleon, leaving the K traveling sharply backwards or forwards in the center of momentum system. A similar stripping of the K will produce an even sharper peaking of the hyperon. Our experiment, however, can only identify the upstream K^0 peak.

IX. ACKNOWLEDGMENTS

Among the many people at the Lawrence Radiation Laboratory who have helped in completing this experiment, I would particularly like to thank Professor Burton J. Moyer for his valuable advice and guidance, Dr. John Osher for the important part he played in the execution of all parts of this experiment, Gilbert Mead for his help during the Bevatron run, and Don Itzel for preparing the programs for the computer calculations.

Also I would like to thank Harry G. Heard, Dr. Edward Lofgren, and the members of the Bevatron crew for the operation of the Bevatron.

This work was done under the auspices of the U. S. Atomic Energy Commission.

X. APPENDICES

Appendix I. Symbols

The following symbols are used in these Appendices

$c = 1$ = velocity of light

E = total energy

E_1 = a special total energy (See p. 70.)

E_2 = a special total energy (See p. 70.)

$E_{(\beta_x, N)}$ = a special total energy (See p. 69.)

N = total energy in center-of-momentum system

P = momentum (three-vector)

M = mass

β = velocity

$\gamma = (1 - \beta^2)^{-1/2}$

$\bar{\beta}$ = velocity of center of momentum

$\bar{\gamma} = (1 - \bar{\beta}^2)^{-1/2}$

β_x = velocity of nucleon projected on beam direction

d = distance along particle path

r = projection of d on horizontal plane

τ = proper lifetime

α = angle from beam direction in horizontal plane

θ = polar angle measured from beam direction

ϕ = azimuthal angle around beam direction

Θ = angle between unstable-particle momentum and subsequent-decay γ momentum

$|M|^2$ = matrix element squared

F = phase-space factor

G = density of particles as a function of the quantity in the subscript

N_γ = final gamma counting rate

n = number of γ rays per decay

b = branching ratio for decay into one or more neutral pions

j = parameter in matrix element

k = parameter in matrix element

t = normalization factor (See p. 70.)

$g = 1.725$

$h = 33.924$

Subscripts which may be added to the above quantities are:

Particle subscripts (capitalized and come first)	Reference-frame subscripts (in small letters and come second)
T = entire system	ℓ = lab frame
K = K particle } U = unstable particle (K or Y)	c = center of momentum
	k = K frame
Y = hyperon }	y = Y frame
$\pi^0 = \pi^0$ meson	u = U frame
I = incident nucleon	$\pi^0 = \pi^0$ frame
F = target nucleon	
N = final-state nucleon	

If a coordinate is to be added, it will come after the reference-frame subscript and be preceded by a comma, e.g., $P_{U\ell, r}$ is the momentum of an unstable particle in laboratory frame along the r direction. This will not be used frequently (fortunately).

Appendix II. Derivation of Integral for Calculated Counting Efficiency

Before the factor of physical significance--the effective matrix elements for strange-particle production--can be found from the experimental data, the effect of three other factors must be unfolded: the kinematics of the decay chain, the geometrical and energy efficiency of the counter telescope, and the phase-space factor. This is done by:

(a) Assuming a specific form for the matrix element.

(b) Multiplying by the phase-space factor.

(c) Calculating the velocity of the center of momentum, the energy in this system, and the relative probability of this value of the energy in order to transform to the laboratory system.

(d) Transforming to the laboratory system in order to find the probability that the unstable particle will enter the volume viewed by the collimation. (See Fig. 15 for the effect of such a transformation on a typical set of particle momenta.)

(e) Further multiplying by the probability that it will decay within that volume.

(f) Multiplying by the probability that γ rays will be created in the decay.

(g) Multiplying by the probability that one will enter the solid angle of the counter.

(h) Multiplying by the probability that it will count when it arrives.

Each of these is calculated for specific decay γ-ray energies, U center-of-momentum azimuthal angle, U polar angles, U energies, and center-of-momentum total energies. An integration is then performed over these variables for each slit position used in the experiment. This is done for all particles that may contribute to the γ counting rate: Λ^0 and Σ^+ downstream from the target and $K^{+,\,-,\,0}$ particles upstream and downstream. The assumptions on the form of the matrix element and the relative numbers of Λ^0, Σ^+, and $K^{+,\,-,\,0}$

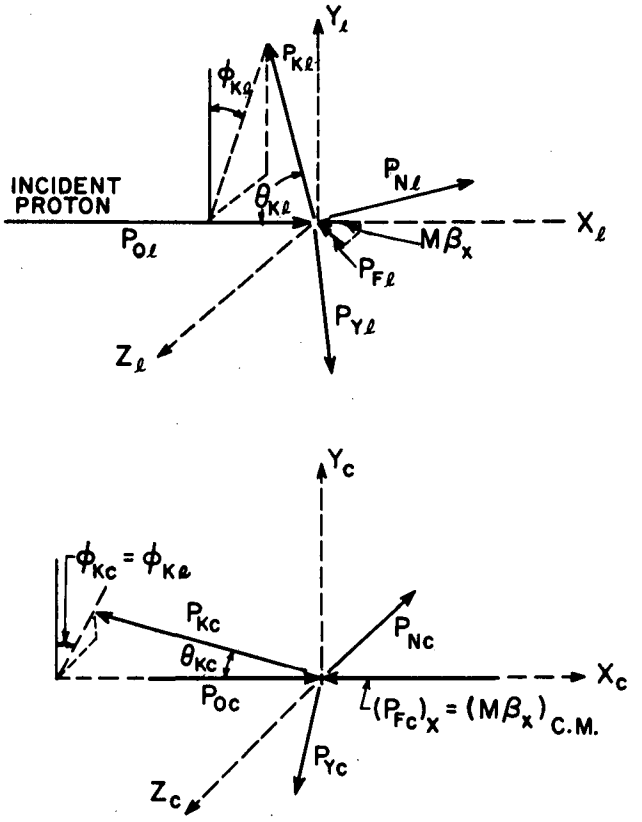

Fig. 15. Typical production schematic for $p+n \rightarrow n+Y+K$. Top: laboratory system. Bottom: center-of-momentum system.

particles are varied to give a best fit with the data and then varied further to determine the range of variation compatible with experiment. The presence of a statistical factor of course does not mean that the statistical theory of production is assumed. Here the matrix element is not assumed to be constant.

1. Matrix Element

The matrix element for the production of one of the particles in the basic reaction analyzed,

$$P + \text{nucleon} \rightarrow \text{nucleon} + \text{hyperon} + K \text{ meson},$$

can be described as

$$|M|^2 = f(P_{Uc}, \theta_{Uc}) = \sum_j \sum_k a_{jk} (P^2_{Uc})^j \cos^k \theta_{Uc}. \qquad (1)$$

2. Phase Space

The three-body Fermi phase-space factor conserving energy and momentum but not angular momentum is:[18]

$$F(N, E_{Kc}) = \frac{P_{Kc} E_{Kc}}{6(2\pi)^4 \hbar^6} \left\{ 1 - \frac{2(M_Y^2 + M_N^2)}{(N-E_{Kc})^2 - P_{Kc}^2} + \left[\frac{M_Y^2 - M_N^2}{(N-E_{Kc})^2 - P_{Kc}^2} \right]^2 \right\}^{\frac{1}{2}}$$

$$\left\{ 3(N-E_{Kc})^2 \left[1 - \left(\frac{M_Y^2 - M_N^2}{(N-E_{Kc})^2 - P_{Kc}^2} \right)^2 \right] - P_{Kc}^2 \left[1 - \frac{2(M_Y^2 + M_N^2)}{(N-E_{Kc})^2 - P_{Kc}^2} + \left(\frac{M_Y^2 - M_N^2}{(N-E_{Kc})^2 - P_{Kc}^2} \right)^2 \right] \right\} \qquad (2)$$

Here $F(N, E_{Yc})$ and $F(N, E_{Nc})$ may be obtained from Eq. (2) by interchange of the subscripts Yc and Kc for the first and Nc and Kc for the second. In general it will be referred to as $F(N, E_{Uc})$.

Because other phase-space factors or combinations of factors may enter, such as the Lepore-Neuman phase space in which high-energy particles have slightly less phase space,[19] or a four-body phase space, the experiment more properly can be thought of as

determining $|M|^2 F(N, E_{Uc})$. Determining $|M|^2$ assuming other phase space models however does not require a repetition of the kinematics calculations which involve the use of an IBM 704. It is only necessary to set

$$|M'|^2 = M^2 \frac{F}{F'} \pm (\text{error assigned to } |M|^2) \frac{F}{F'},$$

at all energies. (This is exactly true only if the maximum-energy K particle from the process associated with M' is the same as from $N + N \rightarrow Y + K + N$. For such processes as $N + N \rightarrow Y + K + N + 1$ or 2π this is still a good assumption.)

3. Center-of-Momentum Velocity, Center-of-Momentum Energy

A Fermi distribution of target-nucleon momenta is assumed. Previous computer work on a similar problem has shown that the use of a Gaussian momentum distribution ($\sim p^2 e^{-p^2/p0^2}$) does not alter the results significantly. The beam-energy distribution can be found from the slope of the monitoring induction-electrode signal and was essentially constant from 6.0 to 6.2 Bev and zero elsewhere. From this we may find the velocity of the center of momentum and the probability of having a system with total energy N in the center of momentum. The Fermi distribution is:

$$G_{F\ell} dP_{F\ell} = \text{density of nucleons with momentum } P_{F\ell} \qquad (3)$$

where we have for $P_{F\ell} \leq P_{F\ell}^{max}$,

$$G_{F\ell}\, dP_{F\ell} = (\text{const.}) P^2_{F\ell}\, dP_{F\ell}$$

and for $P_{F\ell} > P_{F\ell}^{max}$,

$$G_{F\ell}\, dP_{F\ell} = 0.$$

Defining

$$\beta_x = \text{projected laboratory velocity in x direction,} \qquad (4)$$

$$\beta_x = \frac{P_{F\ell}}{M_N} \cos \theta_{F\ell},$$

and

$$G_{\beta x} = \text{density of nucleons with projected velocity } \beta_x, \qquad (5)$$

we can write immediately

$$G_{\beta x} = \text{const.} \left[(P_{F\ell}^{max})^2 - (M_N \beta_x)^2 \right], \tag{6}$$

because $G_{\beta x}$ will be proportional to the area cut by a sphere of radius $P_{F\ell}^{max}$ on a plane a distance $M_N \beta_x$ from the center of the sphere. Taking a cutoff of $\beta_x^{max} = 0.22$ and normalizing, we obtain

$$G_{\beta x} = 1.725 - 33.924\, \beta_x^2, \text{ for } \beta_x \leq 0.22, \tag{7}$$

and

$$G_{\beta x} = 0 \text{ for } \beta_x > 0.22.$$

Given $\vec{P}_{I\ell}$ and $\vec{P}_{F\ell}$, we can calculate the values of the two quantities dependent on them and needed for the description of the KYN system, the total energy in the center-of-momentum system, N, and the velocity of the center of momentum in the lab, $\bar{\beta}$.

The total energy is

$$N = \left[E_{Tc}^2 - P_{Tc}^2 \right]^{\frac{1}{2}} = \left[E_{T\ell}^2 - P_{T\ell}^2 \right]^{\frac{1}{2}} = \left[(E_{I\ell} + E_{F\ell})^2 - (P_{I\ell}^2 + P_{F\ell}^2 + 2\vec{P}_{I\ell} \cdot \vec{P}_{F\ell}) \right]^{\frac{1}{2}}$$

$$= \left[2M_N^2 + 2E_{I\ell}E_{F\ell} - 2P_{I\ell}P_{F\ell} \cos\theta_{F\ell} \right]^{\frac{1}{2}} . \tag{8}$$

Because we have

$$0 = P_{Tc} = \bar{\gamma} (P_{T\ell} - \bar{\beta} E_{T\ell}),$$

we may write

$$\bar{\beta} = \frac{P_{T\ell}}{E_{T\ell}} = \left[E_{I\ell} + E_{F\ell} \right]^{-1} \left[P_{I\ell}^2 + P_{F\ell}^2 + 2 P_{I\ell} P_{F\ell} \cos\theta_{F\ell} \right]^{\frac{1}{2}} . \tag{9}$$

The use of these expressions as they stand would require integration over both $P_{F\ell}$ and $P_{I\ell}$ in addition to later integrations over E_{Kc}, θ_{Kc} ϕ_{Kc}, and $E_{\gamma\ell}$ for calculating a final counting rate. Because computing time is exponentially dependent on the number of integrations, an extra integration is not to be taken lightly; as a matter of fact, in the present case it can't be taken at all. The simplest solution is to consider N as the fundamental variable of integration, weight the integrand by a density function for the number of states as a function of N,

and, consider $\bar{\beta}$ as a constant by neglecting $P_{F\ell}^2$, $2\,P_{I\ell}P_{F\ell}\cos\theta_{F\ell}$, and the kinetic energy part of $E_{F\ell}$. This causes an error of several percent. We can do slightly better than that by substituting the expression for N in that for $\bar{\beta}$, and replacing $E_{I\ell}$ and $E_{F\ell}$ with their average values:

$$\bar{\beta} = \left[1 - \left(\frac{N}{E_{T\ell}}\right)^2\right]^{\frac{1}{2}} = \left[1 - \left(\frac{N}{E_{I\ell}+E_{F\ell}}\right)^2\right]^{\frac{1}{2}} \tag{10}$$

$$\bar{\beta} = \left[1 - \left(\frac{N}{E_{I\ell}^{av}+E_{F\ell}^{av}}\right)^2\right]^{\frac{1}{2}} ,$$

where we have

$$E_{F\ell}^{av} = \left[\int_0^{P_{F\ell}^{max}} E_{F\ell}P_{F\ell}^2\,dP_{F\ell}\right]\left[\int_0^{P_{F\ell}^{max}} P_{F\ell}^2\,dP_{F\ell}\right]^{-1} \cong \frac{3}{5}E_{F\ell}^{max} + \frac{2}{5}M_N, \tag{11}$$

$$E_{F\ell}^{av} = 1.015\,M_N \quad (E_{F\ell} = M_N + P_{F\ell}^2/2M_N \text{ is used here.})$$

and

$$E_{I\ell}^{av} = \frac{1}{2}\left(E_{I\ell}^{min} + E_{I\ell}^{max}\right) = 7.51\,M_N. \tag{12}$$

This gives

$$\bar{\beta} = \left[1 - \frac{N^2}{(8.53)^2 M_N{}^2}\right]^{\frac{1}{2}} = \left[1 - 0.0137\left(\frac{N}{M_N}\right)^2\right]^{\frac{1}{2}} \tag{13}$$

and

$$\bar{\gamma} = \left[1 - \bar{\beta}^2\right]^{-\frac{1}{2}} = \frac{E_{T\ell}}{N} = 8.53\,\frac{M_N}{N}\,. \tag{14}$$

The error in the formula for $\bar{\beta}$ is at most ~ 0.3% compared with ~ 3% for the $\bar{\beta}$ = constant approximation, and its use does not require an extra integration.

To find the distribution for the number of collisions as a function of N, we start from the expression for the number of nucleons as a function of projected velocity,

$$G_{\beta_x} = g - h\beta_x$$

for $\beta_x \leq 0.22$, g = 1.725, and h = 33.924, and

$$G_{\beta_x} = 0 \tag{7}$$

for $\beta_x > 0.22$,

and the number of beam protons as a function of the laboratory energy,

$$G_{E_{I\ell}} = [\,0.22\, M_N]^{-1} \text{ in the limits } 7.40 \leq \frac{E_{I\ell}}{M_N} \leq 7.62. \tag{15}$$

Each state can be represented by a point in a β_x - $E_{I\ell}$ plane with the z axis representing the product of G_{β_x} and $G_{E_{I\ell}}$, the probability of that state (Fig. 16).
Lines of constant N can be drawn on the β_x - $E_{I\ell}$ plane (five sample lines are shown). The probability of finding a system with energy N is proportional to the integral of $G_{\beta_x}\, G_{E_{I\ell}}$ taken along the line N within the rectangle

$$-0.22 \leq \beta_x \leq 0.22,\ 7.40 \leq \frac{E_{I\ell}}{M_N} \leq 7.62.$$

To write this integral we need formulas (16), (17), and (18):

$$N = [2M_N^2 + 2\, E_{I\ell}E_{F\ell} - 2\, P_{I\ell}M_N\beta_x]^{\frac{1}{2}} \tag{16}$$

$$\beta_x = \frac{2\,M_N^2 + 2E_{I\ell}E_{F\ell} - N^2}{2\,P_{I\ell}\,M_N} \cong \frac{2\,M_N^2 + 2E_{I\ell}^{av}\,E_{F\ell}^{av} - N^2}{2\,P_{I\ell}^{av}\,M_N} \tag{17}$$

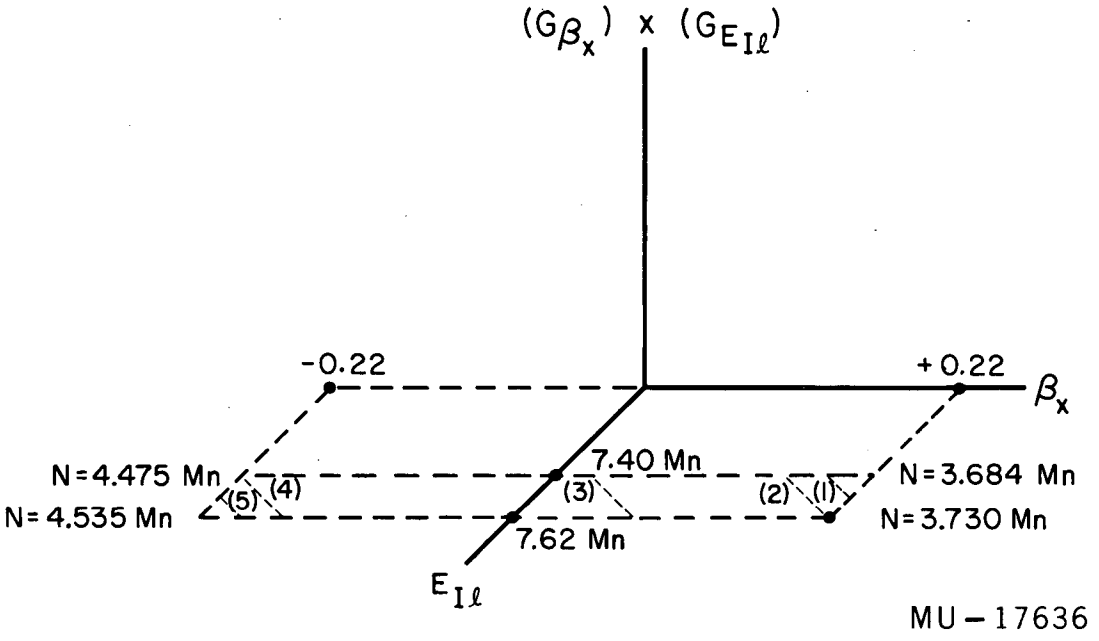

Fig. 16. Calculation of G_N.

It will now be useful to express the incident energy in the laboratory in terms of β_x and N:

$$E(\beta_x, N) \equiv E_I$$

such that a beam proton of this energy and a nucleon of projected velocity β_x produces a system of center-of-momentum energy N. The energy $E(\beta_x, N)$ as a function of β_x will give the lines of constant N). Using

$$N = \left[2M_N^2 + 2E_{I\ell}E_{F\ell}^{av} - 2P_{I\ell}M_N\beta_x\right]^{\frac{1}{2}}, \tag{16}$$

$$(N^2-2M_N^2 - 2E_{I\ell}E_{F\ell}^{av})^2 = 4M_N^2\beta_x^2(E_{I\ell}^2 - M_N^2),$$

$$E_{I\ell}^2(4E_{F\ell}^{av\,2} - 4M_N^2\beta_x^2) + 4E_{F\ell}^{av}E_{I\ell}(2M_N^2 - N^2) + (N^2 - 2M_N)^2 + 4M_N^4\beta_x^2 = 0,$$

$$E(\beta_x, N) \equiv E_{I\ell} = \left\{4E_{F\ell}^{av}(N^2-2M_N^2) + \left[16E_{F\ell}^{av\,2}(N^4-4N^2M_N^2+4M_N^4) - \right.\right.$$

$$\left.\left. -4(4E_{F\ell}^{av\,2} - 4M_N^2\beta_x^2)(N^4-4N^2M_N^2+4M_N^4+4M_N^4\beta_x^2)\right]^{\frac{1}{2}}\right\} \Big/ 8(E_{F\ell}^{av\,2} - M_N^2\beta_x^2),$$

and

$$E(\beta_x, N =$$

$$\frac{E_{F\ell}^{av}(N^2-2M_N^2) + [M_N^2\beta_x^2(N^4-4N^2M_N^2+4M_N^4+4M_N^4\beta_x^2) - E_{F\ell}^{av\,2}M_N^4\beta_x^2(4)]^{\frac{1}{2}}}{2(E_{F\ell}^{av\,2} - M_N^2\beta_x^2)}$$

we get

$$E(\beta_x, N) = \frac{E_{F\ell}^{av}(N^2-2M_N^2) + M_N\beta_x[(N^2-2M_N^2)^2 + 4M_N^2(M_N^2\beta_x^2 - E_{F\ell}^{av\,2})]^{\frac{1}{2}}}{2(E_{F\ell}^{av\,2} - M_N^2\beta_x^2)}. \tag{18}$$

Then we may write

$$G_N = t \int_{E_1}^{E_2} \int_{-0.22\,M_N}^{0.22\,M_N} G_{\beta_x} G_{E_{I\ell}} \delta(N - [2M_N^2 + 2E_{I\ell}E_{F\ell}^{av} - 2P_{I\ell}M_N\beta_x]^{\frac{1}{2}}) \, d(M_N\beta_x)dE_{I\ell}, \tag{19}$$

where δ is the Dirac δ function and t is a normalization constant to be determined later. The limits E_1, E_2 are set as follows:

$$\begin{aligned}
&13.574 \leq \left(\frac{N}{M_N}\right)^2 \leq 13.916 \qquad E_1 = 7.40\,M_N \qquad E_2 = E(0.22, N) \\
&13.916 \leq \left(\frac{N}{M_N}\right)^2 \leq 20.026 \qquad E_1 = 7.40\,M_N \qquad E_2 = 7.62\,M_N \\
&20.026 \leq \left(\frac{N}{M_N}\right)^2 \leq 20.564 \qquad E_1 = E(-0.22, N) \qquad E_2 = 7.62\,M_N .
\end{aligned} \tag{20}$$

The first set of limits apply to an integration path along a line of constant N such as in Eq. (1). For the paths of Eqs. (2), (3), and (4) the second set of limits apply. For a path such as that of Eq. (5), the third set applies. Performing the first integration and using Eq. (17), we obtain:

$$G_N = t \int_{E_1}^{E_2} \left[g - h\left(\frac{2M_N^2 + 2E_{I\ell}E_{F\ell}^{av} - N^2}{2P_{I\ell}\,M_N} \right)^2 \right] \frac{1}{0.22M_N} \, dE_{I\ell}$$

$$G_N = \frac{t}{0.22\ M_N}\left[g\int_{E_1}^{E_2} dE_{I\ell} - h\int_{E_1}^{E_2} \frac{(2M_N^2 - N^2)^2}{4M_N^2(E_{I\ell}^2 - M_N^2)}\ dE_{I\ell}\right.$$

$$\left. - h\int_{E_1}^{E_2} \frac{(2M_N^2 - N^2)}{4M_N^2} \cdot \frac{2(2E_{F\ell}^{av})E_{I\ell}\,dE_{I\ell}}{E_{I\ell}^2 - M_N^2} - h\int_{E_1}^{E_2} \left(\frac{2E_{F\ell}^{av}}{2M_N}\right)^2 \frac{E_{I\ell}^2}{E_{I\ell}^2 - M_N^2}\ dE_{I\ell}\right]$$

$$G_N = \frac{t}{0.22\ M_N}\left[g(E_2 - E_1) - \frac{h(2M_N^2 - N^2)}{4M_N^2}\int_{E_1}^{E_2} \frac{dE_{I\ell}}{E_{I\ell}^2 - M_N^2}\right.$$

$$\left. - \frac{h(E_{F\ell}^{av})}{M_N^2}(2M_N^2 - N^2)\int_{E_1}^{E_2} \frac{E_{I\ell}\,dE_{I\ell}}{E_{I\ell}^2 - M_N^2} - \frac{h(E_{F\ell}^{av})^2}{M_N^2}\int_{E_1}^{E_2} \frac{E_{I\ell}^2\,dE_{I\ell}}{E_{I\ell}^2 - M_N^2}\right]$$

$$G_N = \frac{t}{0.22\ M_N}\left\{g(E_2 - E_1) + \frac{h(2M_N^2 - N^2)^2}{4M_N^2}\ \frac{1}{2M_N}\ \ln\frac{M_N + E_{I\ell}}{-M_N + E_{I\ell}}\ \right|_{E_1}^{E_2}$$

$$\left. - \frac{h(E_{F\ell}^{av})}{2M_N^2}(2M_N^2 - N^2)\ln\frac{E_2^2 - M_N^2}{E_1^2 - M_N^2} - \frac{h(E_{I\ell}^{av})}{M_N^2}\left[E_{I\ell} - \frac{M_N}{2}\ln\frac{M_N + E_{I\ell}}{-M_N + E_{I\ell}}\right]\right|_{E_1}^{E_2}\Bigg\}$$

$$G_N = \frac{t}{0.22\,M_N}\left\{g(E_2-E_1)+\frac{h(2M_N^2-N^2)^2}{8M_N^3}\ln\frac{E_2+M_N}{E_2-M_N}\cdot\frac{E_1-M_N}{E_1+M_N}\right.$$

$$\left.-\frac{hE_{F\ell}^{av}(2M_N^2-N^2)}{2M_N^2}\cdot\ln\frac{E_2^2-M_N^2}{E_1^2-M_N^2}-\frac{h(E_{F\ell}^{av})^2}{M_N^2}\left[E_2-E_1+\frac{M_n}{2}\ln\frac{E_2-M_N}{E_2+M_N}\cdot\frac{E_1+M_N}{E_1-M_N}\right]\right\}$$

$$G_N = N^4\left[\frac{ht}{(0.22M_N^4)}\frac{1}{8}\ln\frac{E_2+M_N}{E_2-M_N}\cdot\frac{E_1-M_N}{E_1+M_N}\right]+N^2\left[\frac{-t(4M_N^2)h}{8(0.22)M_N^4}\cdot\right.$$

$$\left.\ln\frac{E_2+M_N}{E_2-M_N}\cdot\frac{E_1-M_N}{E_1+M_N}+\frac{ht\,E_{F\ell}^{max}}{0.44\,M_N^3}\ln\frac{E_2^2-M_N^2}{E_1^2-M_N^2}\right]$$

$$+\left[\frac{gt(E_2-E_1)}{0.22\,M_N}+\frac{ht\,4M_N^4}{8(0.22)M_N^4}\ln\frac{E_2+M_N}{E_2-M_N}\,\frac{E_1-M_N}{E_1+M_N}\right.$$

$$\left.-\frac{ht\,E_{F\ell}^{av}}{2(0.22)}\frac{(2M_N^2)}{M_N^3}\ln\frac{E_2^2-M_N^2}{E_1^2-M_N^2}-\frac{ht(E_{F\ell}^{max})^2}{0.22\,M_N^3}\left\{E_2-E_1+\frac{M_N}{2}\ln\frac{E_2-M_N}{E_2+M_N}\cdot\frac{E_1+M_N}{E_1-M_N}\right\}\right]$$

$$G_N = \left(\frac{N}{M_N}\right)^4 \left[\frac{ht}{8(0.22)} \ln \frac{E_2+M_N}{E_2-M_N} \frac{E_1-M_N}{E_1+M_N}\right] + \tag{21}$$

$$\left(\frac{N}{M_N}\right)^2 \left[\frac{ht(E_{F\ell}^{av})}{2(0.22)M_N} \ln \frac{E_2^2-M_N^2}{E_1^2-M_N^2} - \frac{ht}{2(0.22)} \ln \frac{E_2+M_N}{E_2-M_N} \frac{E_1-M_N}{E_1+M_N}\right] +$$

$$\left[(E_2-E_1)\left(\frac{gt}{0.22M_N} - \frac{ht(E_{F\ell}^{av})^2}{0.22\,M_N^3}\right) + \left(\frac{-1}{2(0.22)} - \frac{(E_{F\ell}^{av})^2}{2(0.22)M_N^2}\right)\right] \cdot$$

$$\left(ht \ln\left(\frac{E_2-M_N}{E_2+M_N}\right)\left(\frac{E_1+M_N}{E_1-M_N}\right)\right) - \frac{ht\,E_{F\ell}^{av}}{0.22\,M_N} \ln \frac{E_2^2-M_N^2}{E_1^2-M_N^2}\Bigg] .$$

For $3.730\,M_N \leq N \leq 4.475\,M_N$ this reduces to

$$G_N = t\left[-0.153103\left(\frac{N}{M_N}\right)^4 + 5.28024\left(\frac{N}{M_N}\right)^2 - 43.8041\right] . \tag{22}$$

A numerical evaluation of Eq. (22) in the more complicated upper and lower regions $3.684\,M_N \leq N \leq 3.730\,M_N$ and $4.475\,M_N \leq N \leq 4.535\,M_N$ shows that it does not differ much from Eq. (22) extended beyond its upper and lower limits because both are small compared with middle-range values of Eq. (22). With less than 0.2% error in the final answer, it is possible to use, for $3.727\,M_N \leq N \leq 4.538\,M_N$,

$$G_N = -0.164586\left(\frac{N}{M_N}\right)^4 + 5.67628\left(\frac{N}{M_N}\right)^2 - 47.0895, \qquad (22')$$

and, for $4.538\ M_N \leq N \leq 3.727\ M_N$,

$$G_N = 0.$$

4. Probability for Entering the Viewed Area

The requirement that the unstable particle enter the volume viewed by the telescope is used to set the limits on the second and third integrations, those over ϕ_c and θ_c. This will be reduced to a probability when it is divided by the normalization integral. The volume is determined by two identical slits, one above the other, with two sides concentric circles centered on the target and two sides radial lines. Any point within the column determined by these slits will see the full solid angle of the slit system ($\sim 10^{-4}$), all of it essentially at $\theta_1 = 90^o$, $\phi = 0^o$ and independent to within about 1% of the exact vertical position of the particle path. For points outside but adjacent to this volume, θ_c and ϕ are still essentially unchanged, but the solid angle goes to zero over a distance that is not small compared with the dimensions of the slits. In order to calculate the contribution of these regions to the counting rate, the solid angle viewed from them was computed as a function of position. Because it cannot be expressed in a simple closed form, it was not left inside the integral but was replaced with a series of step functions for each subdivision of the viewed region bounded by concentric cylinders and radial planes.

The integration over ϕ can be split in two ranges, one in which the cone of half angle θ_1 intersects the sides of the viewed region above the horizontal plane, and one below it. It can be seen from Fig. 17 (I hope) that the limits on ϕ are:

Range 1.

For $0 \leq \theta_\ell \leq \frac{\pi}{2}$, we have

$$\sin \phi_{min} = \frac{\tan \alpha_1}{\tan \theta_\ell}. \qquad (23)$$

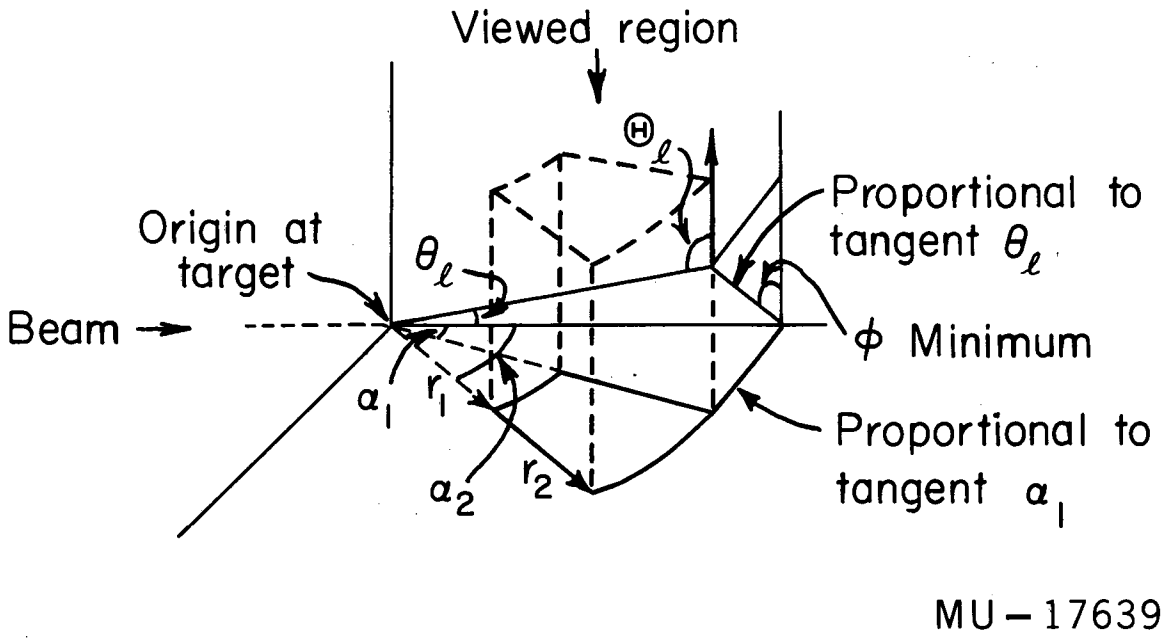

Fig. 17. Quantities involved in limits of angular integrations.

If $\frac{\tan \alpha_1}{\tan \theta_\ell}$ is less than 0 or greater than 1, the ϕ integral will be zero because the cone does not intersect the viewed volume and

$$\sin \phi_{max} = \frac{\tan \alpha_2}{\tan \theta_\ell} \quad .$$

(If $\frac{\tan \alpha_2}{\tan \theta_\ell}$ is less than zero or greater than 1, ϕ_{max} equals $\frac{\pi}{2}$, because the cone does not reach the far side of the viewed volume.)

For $\frac{\pi}{2} \leq \theta_\ell \leq \pi$, we have

$$\sin \phi_{min} = \frac{\tan \alpha_2}{\tan \theta_\ell} \quad .$$

(If $\sin \phi_{min}$ is less than 0 or greater than 1, the ϕ integral will be zero.)

and

$$\sin \phi_{max} = \frac{\tan \alpha_1}{\tan \theta_\ell} \quad .$$

(If $\sin \phi_{max}$ is less than 0 or greater than 1, then $\phi_{max} = \frac{\pi}{2}$.)

Range 2.

In this range we have

$$\phi_{min}' = \pi - \phi_{max} \tag{24}$$

and

$$\phi_{max}' = \pi - \phi_{min} .$$

It is assumed that we have $0 \leq \alpha_1 < \alpha_2 \leq \pi$. The integral will not need to be computed for other values because of its right-left symmetry.

If hyperons were strongly polarized in production, retained this polarization in escaping from the Ta nucleus, and contributed significantly to the counting rate through their π^0-plus-nucleon decay, a right-left asymmetry would exist. Such an asymmetry was looked for but was not seen, among other possible reasons because of the much higher counting rate from $K_1^0 \rightarrow \pi^0 + \pi^0$. For purposes of estimating the maximum possible hyperon contribution to the observed counting rate, it is assumed that the decays are isotropic in the hyperon rest frame.

The limits on θ_ℓ are fairly simply expressed. Because we need θ_c^{min} and θ_c^{max} for the integrals, we solve

$$\cot\theta_\ell = \bar{\gamma}\left(\cot\theta_c + \frac{\bar{\beta}}{\beta_c}\csc\theta_c\right) \tag{25}$$

for θ_c, getting

$$\theta_c^{\pm}(\theta_\ell) = \cot^{-1}\left[\bar{\gamma}\left(1-\frac{\bar{\beta}}{\beta_c^2}\right)\right]^{-1}\left\{\cot\theta_\ell \pm \frac{\bar{\beta}}{\beta_c}\left[\cot^2\theta_\ell + \bar{\gamma}^2\left(1-\frac{\bar{\beta}^2}{\beta_c^2}\right)\right]^{\frac{1}{2}}\right\}. \tag{26}$$

Here the + sign is used for those cases where a particle heading backwards in the center-of-momentum system comes out forward in the laboratory system. Then the limits on θ_c are as shown in Table IV.

Table IV

Limits on θ_c (27)

Slit position	$\beta_c > \bar{\beta}$		$\beta_c \leq \bar{\beta}$ [a]	
	θ_c^{min}	θ_c^{max}	θ_c^{min}	θ_c^{max}
$0 \leq a_1 < a_2 < \frac{\pi}{2}$	$\theta_c^-(a_1)$	$\theta_c^-(\frac{\pi}{2})$	$\theta_c^-(a_1)$	$\theta_c^+(a_1)$
$0 \leq a_1 \leq \frac{\pi}{2} \leq a_2 \leq \pi$	$\theta_c^-(a_1)$	$\theta_c^-(a_2)$	$\theta_c^-(a_1)$	$\theta_c^+(a_1)$
$\frac{\pi}{2} \leq a_1 < a_2 \leq \pi$	$\theta_c^-(\frac{\pi}{2})$	$\theta_c^-(a_2)$	—	—

[a] For $\cot^2\theta_\ell \leq \bar{\gamma}^2\left(1-\frac{\bar{\beta}^2}{\beta_c^2}\right)$, this value of θ_c does not contribute to the counting rate because all particles come out in a cone whose central angle is too small to intercept the viewed region; therefore set the θ integrand involved to zero.

5. Exponential Decay Factor

The probability that the particle will decay within the viewed region is given by

$$\exp\left[-\frac{\text{proper time to reach r}}{\tau}\right]\Bigg|_{r_2}^{r_1} = \exp\left[-\frac{\text{lab time}}{\gamma_\ell\,\tau_U}\right]\Bigg|_{r_2}^{r_1}$$

$$= \exp\left[-\frac{d}{\beta_\ell\,\gamma_\ell\,\tau_U}\right]\Bigg|_{r_2}^{r_1}$$

$$= \exp\left[-\frac{M_U}{P_\ell\,\tau_U}\right]\Bigg|_{r_2}^{r_1} \quad .$$

Because we have $d/P_\ell = r/P_{\ell,r}$ where d is the distance along the particle path, r is the projection of d on a horizontal plane, and $P_{\ell,r}$ is the component of P_ℓ along r.
For

$$P_\ell = \left[\bar{\gamma}^2(P_c\cos\theta_c + \bar{\beta}\,E_c)^2 + P_c^{\,2}\sin^2\theta_c\sin^2\phi\right]^{\frac{1}{2}} \quad ,$$

the decay probability is:

$$\exp\left\{-\frac{M_U r}{c\tau_U P_{Uc}}\left[\bar{\gamma}^2\left(\cos\theta_c + \frac{\bar{\beta}}{\beta_c}\right)^2 + \sin^2\theta_c\sin^2\phi\right]^{\frac{1}{2}}\right\}\Bigg|_{r_2}^{r_1} \quad . \qquad (28)$$

The velocity of light c is here (and only here) inserted explicitly so that the distance r can be given in centimeters rather than light seconds.

6. Number of γ rays per Decay

The number of γ's created per decay is written as nb where n is the number per neutral decay (2 for the Λ^0, $K^{\pm}$ and Σ^+, 4 for the K^0) and b is the branching ratio.

7. Probability of Detection of the Gamma Ray

It is necessary to know the spectrum and angular distribution of the decay γ rays before the probability of their entering the solid angle of the counter and counting on arrival can be calculated. When a K decays the pions will have an isotropic angular distribution because the K^0 is a zero-spin particle. The π mesons from Λ^0 and Σ^+ decay will also be isotropic if the Λ^0 and Σ^+ are not polarized. In any event, this assumption will be made for the reasons mentioned in Section 4. The γ rays from the π^0 decay are isotropic and mono-energetic in the π^0 frame. In the K, Λ^0, or Σ^+ frame (in general, referred to as the u frame) they have the usual "rectangular" spectrum. A constant number per unit energy interval from the minimum energy of

$$E_{\gamma u}^{min} = \gamma_{\pi^0 u} \left[E_{\gamma\pi^0} - \beta_{\pi^0 u} P_{\gamma\pi^0} \right] = \frac{1}{2} M_{\pi^0} \gamma_{\pi^0 u} (1 - \beta_{\pi^0 u})$$

to the maximum energy of $1/2\, M_{\pi^0}\gamma_{\pi^0 u}(1+\beta_{\pi^0 u})$. Although the γ rays from π^0 particles traveling in a given direction are not isotropic in the u frame, the neutral pions are, and therefore the total γ flux is still isotropic. Then the probability of the creation of a γ that will count is equal to

$$nb \int_{E_{\gamma u}^{min}}^{E_{\gamma u}^{max}} \int_{\Omega \text{ of slit in u system}} \frac{\epsilon(E_{\gamma \ell})\, dE_{\gamma u}\, d\Omega_{\gamma u}}{M_{\pi^0}\, \gamma_{\pi^0 u} \beta_{\pi^0 u}\, 4\pi}$$

where $\epsilon(E_{\gamma \ell})$ is the efficiency of the γ telescope, 4π is the normalization factor for the solid-angle integration, and $E_{\gamma u}^{max} - E_{\gamma u}^{min} = M_{\pi^0}\gamma_{\pi^0 u}\beta_{\pi^0 u}$ is the normalization factor for the energy integration. In order to carry out this integration it is necessary to transform to the laboratory system. The normalization factors are constants and will not change providing the proper Jacobian is used. Three things must now be found:

(a) the gamma-energy transformation for the limits of the energy integral

(b) the angle Θ_ℓ between the U direction in the laboratory and the vertical

(c) the Jacobian allowing the replacement of $dE_{\gamma u}\ d\Omega_{\gamma u}$ with $dE_{\gamma \ell}\ d\Omega_{\gamma \ell}$.

(a) Energy transformation. We use here the expression

$$E^{max}_{\gamma u} = \gamma_{U\ell}\left(E^{max}_{\gamma \ell} - \beta_{U\ell} P^{max}_{\gamma \ell} \cos\Theta_\ell\right)$$

$$E^{max}_{\gamma \ell} = E^{max}_{\gamma u}\left[\gamma_{U\ell}(1-\beta_{U\ell}\cos\Theta_\ell)\right]^{-1} = \frac{M_{\pi 0}\gamma_{\pi 0 u}(1+\beta_{\pi 0 u})}{2\gamma_{U\ell}(1-\beta_{U\ell}\cos\Theta_\ell)}$$

rather than

$$E^{max}_{\gamma \ell} = \gamma_{U\ell}\left(E^{max}_{\gamma u} + \beta_{U\ell} P^{max}_{\gamma u} \cos\Theta_u\right) \qquad (29)$$

because Θ_u is not independent of the gamma energy. Note that $E^{max}_{\gamma \ell}$ is not the maximum energy a gamma may have in the laboratory system, but the maximum a gamma traveling vertically upwards may have. Similarly we have

$$E^{min}_{\gamma \ell} = E^{min}_{\gamma u}\left[\gamma_{U\ell}(1-\beta_{U\ell}\cos\Theta_\ell)\right]^{-1} = \frac{M_{\pi 0}\gamma_{\pi 0 u}(1-\beta_{\pi 0 u})}{2\gamma_{U\ell}(1-\beta_{U\ell}\cos\Theta_\ell)}. \qquad (30)$$

(b) Θ_ℓ. From Fig. 17 it can be seen that $\cos\Theta_\ell = \sin\theta_\ell \cos\phi$. Then we can write

$$\gamma_{U\ell}(1-\beta_{U\ell}\cos\Theta_\ell) = \frac{E_{U\ell}}{M_U} - \frac{P_{U\ell}\cos\Theta_r}{M_U} = \frac{E_{U\ell}}{M_U} - \frac{P_{U\ell,z}}{M_U} \qquad (31)$$

$$= \frac{E_{U\ell}}{M_U} - \frac{P_{Uc,z}}{M_U} = \frac{\bar{\gamma}(E_{Uc} + \bar{\beta} P_{Uc}\cos\theta_c) - P_{Uc}\sin\theta_c\cos\phi_c}{M_U}.$$

(c) The Jacobian. From

$$\iint dE_{\gamma u}\, d\Omega_u = \iiint dE_{\gamma u}\, d(\cos\Theta_u)\, d\phi$$

we obtain, using the following theorem of calculus,

$$\iint dx'\, dy' = \iint \left[\frac{dx'}{dx}\,\frac{dy'}{dy} - \frac{dx'}{dy}\,\frac{dy'}{dx} \right] dx\, dy. \qquad (32)$$

the expression below;

$$\iint dE_{\gamma u}\, d(\cos\Theta_u) = \iint \left[\frac{dE_{\gamma u}}{dE_{\gamma \ell}}\,\frac{d(\cos\Theta_u)}{d(\cos\Theta_\ell)} - \frac{dE_{\gamma u}}{d(\cos\Theta_\ell)}\,\frac{d(\cos\Theta_u)}{dE_{\gamma \ell}} \right] dE_{\gamma \ell}\, d(\cos\Theta_\ell)$$

where $d(\cos\Theta_u)/dE_{\gamma\ell}$ equals 0.

That we have

$$\frac{d}{dE_{\gamma\ell}}(\cos\Theta_u) = 0$$

can be seen from inspection of the formula for $\cos\Theta_u$. Here $\beta_{\gamma\ell}$ ($\equiv 1$), but not $E_{\gamma\ell}$, enters into the equation. Taking the derivative of $E_{\gamma u}$ with respect to $E_{\gamma\ell}$, we have

$$\frac{dE_{\gamma u}}{dE_{\gamma\ell}} = \frac{d}{dE_{\gamma\ell}} \left[\gamma_{U\ell}\, E_{\gamma\ell}\, (1-\beta_{U\ell}\,\beta_{\gamma\ell}\cos\Theta_\ell) \right] = \gamma_{U\ell}(1-\beta_{U\ell}\cos\Theta_\ell).$$

We next find an expression for $\cos\Theta_u$:

$$\left[\frac{\cos^2\Theta_u}{1-\cos^2\Theta_u} \right]^{\frac{1}{2}} = \cot\Theta_u = \gamma_{U\ell}\left(\cot\Theta_\ell - \frac{\beta_{U\ell}}{\beta_{\gamma\ell}}\csc\Theta_\ell\right) = \frac{\gamma_{U\ell}\left(\cos\Theta_\ell - \frac{\beta_{U\ell}}{\beta_{\gamma\ell}}\right)}{\sin\Theta_\ell}$$

$$\cos\Theta_u = \gamma_{U\ell}\left(\cos\Theta_\ell - \frac{\beta_{U\ell}}{\beta_{\gamma\ell}}\right) \left[\sin^2\Theta_\ell - \gamma_{U\ell}^2\left(\cos\Theta_\ell - \frac{\beta_{U\ell}}{\beta_{\gamma\ell}}\right)^2 \right]^{\frac{1}{2}}$$

Taking the derivative of $\cos\Theta_u$ with respect to $\cos\Theta_\ell$, we have

$$\frac{d(\cos\Theta_u)}{d(\cos\Theta_\ell)} = \frac{\gamma_{U\ell}\left[\sin^2\Theta_\ell + \gamma^2_{U\ell}\left(\cos\Theta_\ell - \frac{\beta_{U\ell}}{\beta_{\gamma\ell}}\right)^2\right]}{\left[\sin^2\Theta_\ell + \gamma^2_{U\ell}\left(\cos\Theta_\ell - \frac{\beta_{U\ell}}{\beta_{\gamma\ell}}\right)^2\right]^{\frac{3}{2}}}$$

$$- \frac{\gamma_{U\ell}\left(\cos\Theta_\ell - \frac{\beta_{U\ell}}{\beta_{\gamma\ell}}\right)\left(\frac{1}{2}\right)2\gamma^2_{U\ell}\left(\cos\Theta_\ell - \frac{\beta_{U\ell}}{\beta_{\gamma\ell}}\right)}{\left[\sin^2\Theta_\ell + \gamma^2_{U\ell}\left(\cos\Theta_\ell - \frac{\beta_{U\ell}}{\beta_{\gamma\ell}}\right)^2\right]^{\frac{3}{2}}}$$

$$= \frac{\gamma_{U\ell}\left[\sin^2\Theta_\ell + \cos^2\Theta_\ell - \cos\Theta_\ell\,\frac{\beta_{U\ell}}{\beta_{\gamma\ell}}\right]}{\left[\sin^2\Theta_\ell + \gamma^2_{U\ell}\left(\cos\Theta_\ell - \frac{\beta_{U\ell}}{\beta_{\gamma\ell}}\right)^2\right]^{\frac{3}{2}}}$$

$$= \frac{\gamma_{U\ell}\left[1 - \beta_{U\ell}\cos\Theta_\ell\right]}{\left[\sin^2\Theta_\ell + \gamma^2_{U\ell}(\cos\Theta_\ell - \beta_{U\ell})^2\right]^{\frac{3}{2}}}$$

$$= \frac{\gamma_{U\ell}\left[1 - \beta_{U\ell}\cos\Theta_\ell\right]}{\left[\sin^2\Theta_\ell + \gamma^2_{U\ell}(1-\sin^2\Theta_\ell) - 2\gamma_{U\ell}\beta_{U\ell}\cos\Theta_\ell + \gamma^2_{U\ell}\beta^2_{U\ell}\right]^{\frac{3}{2}}}$$

$$= \frac{\gamma_{U\ell}\,(1 - \beta_{U\ell}\cos\Theta_\ell)}{\left[\gamma^2_{U\ell} + \sin^2\Theta_\ell(1-\gamma^2_{U\ell}) + \gamma^2_{U\ell}\beta^2_{U\ell} - 2\gamma^2_{U\ell}\cos\Theta_\ell\right]^{\frac{3}{2}}}$$

$$= \frac{\gamma_{U\ell}(1-\beta_{U\ell}\cos\Theta_\ell)}{\left[\gamma_{U\ell}^2 + \gamma_{U\ell}^2\,\beta_{U\ell}^2\,(1-\sin^2\Theta_\ell) - 2\gamma_{U\ell}^2\beta_{U\ell}\cos\Theta_\ell\right]^{\frac{3}{2}}}$$

$$= \frac{(1-\beta_{U\ell}\cos\Theta_\ell)}{\gamma_{U\ell}^2\left[1-2\beta_{U\ell}\cos\Theta_\ell+\beta_{U\ell}^2\cos^2\Theta_\ell\right]^{\frac{3}{2}}}$$

$$= \frac{1}{\gamma_{U\ell}^2\,[1-\beta_{U\ell}\cos\Theta_\ell]^2}$$

Combining these we have

$$\iint dE_{\gamma u}\, d\Omega_u = \iint \gamma_{U\ell}\,(1-\beta_{U\ell}\cos\Theta_\ell)\;\frac{dE_{\gamma\ell}\,d\Omega_{\gamma\ell}}{\gamma_{U\ell}^2(1-\beta_{U\ell}\cos\Theta_\ell)^2} \qquad (33)$$

$$= \iint \frac{dE_{\gamma\ell}\,d\Omega_{\gamma\ell}}{\gamma_{U\ell}(1-\beta_{U\ell}\cos\Theta_\ell)} \quad .$$

The resultant probability for the production of a γ that will count is given by

$$nb \int_{\frac{M_{\pi 0}\gamma_{\pi 0_u}(1-\beta_{\pi 0_u})}{2\gamma_{U\ell}(1-\beta_{U\ell}\cos\Theta_\ell)}}^{\frac{M_{\pi 0}\gamma_{\pi 0_u}(1+\beta_{\pi 0_u})}{2\gamma_{U\ell}(1-\beta_{U\ell}\cos\Theta_\ell)}} \frac{\epsilon(E_{\gamma\ell})\,\Delta\Omega_{\gamma\ell}\,dE_{\gamma\ell}}{4\pi\, M_{\pi 0}\gamma_{\pi 0_u}\beta_{\pi 0_u}\;\frac{1}{M_U}\,\gamma_{U\ell}(1-\beta_{U\ell}\cos\Theta_\ell)}$$

where

$$\gamma_{U\ell}\,(1-\beta_{U\ell}\cos\Theta_\ell) = \frac{1}{M_U}\,[\,\bar{\gamma}(E_{Uc}+\bar{\beta}\,P_{Uc}\,\cos\theta_c)-P_{Uc}\sin\theta_c\cos\phi], \tag{31}$$

and the requirement that the γ be directed upwards in the laboratory system has been used in the above relation and in the replacement of the integral over $\Omega_{\gamma\ell}$ by the integrand at that point times $\Delta\Omega_{\gamma\ell}$, the solid angle subtended by the upper slit.

Finally, the integral reduces to

$$\frac{M_U\,\Delta\Omega_{\gamma\ell}\ \text{nb}}{4\pi M_{\pi 0}\,\gamma_{\pi 0_u}\beta_{\pi 0_u}\,\gamma_{U\ell}(1-\beta_{U\ell}\cos\Theta_\ell)}$$

$$\times \int_{\frac{M_{\pi 0}\,\gamma_{\pi 0_u}(1-\beta_{\pi 0_u})}{2\gamma_{U\ell}(1-\beta_{U\ell}\cos\Theta_\ell)}}^{\frac{M_{\pi 0}\,\gamma_{\pi 0_u}(1-\beta_{\pi 0_u})}{2\gamma_{U\ell}(1-\beta_{U\ell}\cos\Theta_\ell)}} \epsilon(E_{\gamma\ell})\,dE_{\gamma\ell}.$$

Collecting the pieces, we obtain the normalized expression for the relative counting rate as a function of position for a given pair of values of i and k:

$$N_\gamma \begin{pmatrix}\text{slit from}\\ r_1 \to r_2\\ a_1 \to a_2\end{pmatrix} = \sum\sum nb \begin{pmatrix}\text{subdivisions}\\ \text{of target}\\ \text{and slit}\end{pmatrix} \int_N G_N \int_{E_{Uc}} F(N_\gamma E_{Uc})[\gamma_{Uc}^2 - 1]^j \int_{\theta_{Uc}} \cos^k\theta_{Uc} \sin\theta_{Uc}$$

(35)

$$\cdot \int_{\phi_{Uc}} \exp\left(-\frac{M_{Ur}}{c\tau_U P_{Uc}}\left[\bar{\gamma}^2(\cos\theta_{Uc} + \frac{\bar{\beta}}{\beta_{Uc}})^2 + \sin^2\theta_{Uc}\sin^2\phi\right]^{-\frac{1}{2}}\right) \Bigg|_{r_2}^{r_1}$$

$$\left\{ \frac{\int_{E_{\gamma\ell}} \epsilon(E_{\gamma\ell})\, dE_{\gamma\ell}\, \Delta\Omega_{\gamma\ell}}{4\pi\beta_{\pi 0_u}\gamma_{\pi 0_u} M_{\pi 0}\gamma_{U\ell}(1-\beta_{U\ell}\cos\Theta_\ell)} \right\} d\phi_{Uc}\, d\theta_{Uc}\, E_{Uc}\, dN.$$

The probability of a γ counting, the factor inside the braces, is already normalized. In order to get a result that will permit a comparison between different values of j and k, it is desirable to normalize the other factors. This is done by dividing by

$$\int_N G_N \int_{E_{Uc}} F(N, E_{Uc})[\gamma_{Uc}^2 - 1]^j \int_{\theta_{Uc}=0}^{\pi} \cos^k\theta_{Uc} \sin\theta_{Uc} \int_{\phi_{Uc}=0}^{2\pi} d\phi_{Uc}\, d\theta_{Uc}\, dE_{Uc}\, dN$$

$$= \frac{4\pi}{k+1} \int_N G_N \int_{E_{Uc}} F(N, E_{Uc})[\gamma_{Uc}^2 - 1]^j\, dE_{Uc}\, dN \qquad (k \text{ even})$$

i.e. the value N_γ would have to within a factor of nb, if all γ rays created were detected.

The limits for all integrations except the E_{Uc} integration have been discussed. For this, the lower limit is of course M_U. The

unstable particle will have its maximum possible energy in the center-of-momentum system when the other two have the maximum momentum consistent with conservation of momentum and the minimum possible energy consistent with that momentum. This will occur when they are moving with the same velocity. Then, for the case in which the K is the unstable particle, we write

$$E_{Kc}^{max} + E_{(Y+N)c} = N$$

$$E_{Kc}^{max\,2} - M_K^2 = E_{(Y+N)}^2 - (M_Y + M_N)^2 = N^2 - 2NE_{Kc}^{max} + E_{Kc}^{max\,2} - (M_Y + M_N)^2$$

$$E_{Kc}^{max} = \frac{1}{2N}\left[N^2 + M_K^2 - (M_Y + M_N)^2\right] .$$

Interchanging the K and Y subscripts will give E_{Yc}^{max} .

8. Summary

A. Integral to be Evaluated

$$N_\gamma = \sum_{\substack{\text{Slit from} \\ r_1 \to r_2,\ a_1 \to a_2}} \sum_{\substack{\text{Subdivisions} \\ \text{of target,} \\ \text{slit}}} inb \; \frac{\int_N G_N \int_{E_{Uc}} F(N, E_{Uc})(P_{Uc}^2)^j \int_{\theta_{Uc}} \cos^k\theta_{Uc} \sin\theta_{Uc} \int_{\phi_{Uc}} \exp\left\{-\frac{M_U^r}{c\tau_U P_{Uc}}\left[\bar\gamma^2(\cos\theta_{Uc} + \frac{\bar\beta}{\beta_{Uc}})^2 + \sin^2\theta_{Uc}\sin^2\phi_U\right]^{-\frac{1}{2}}\right\}\Big|_{r_2}^{r_1}\left[\frac{\int_{E_{\gamma\ell}} \epsilon_\gamma(E_{\gamma\ell})\Delta\Omega_{\gamma\ell}\, dE_{\gamma\ell}\, d\phi_{Uc}\, d\theta_{Uc}\, dE_{Uc}\, dN}{4\pi\beta_{\pi^0\mu}\gamma_{\pi^0\mu} M_{\pi^0}\gamma_{U\ell}(1-\beta_{U\ell}\cos\Theta_\ell)}\right]}{\frac{4\pi}{k+1}\int_N G_N \int_{E_{Uc}} F(N, E_{Uc})(P_{Uc}^2)^j \, dE_{Uc}\, dN}$$

B. Functions to be Calculated for Integral

$G_N = -0.164586\left(\frac{N}{M_N}\right)^4 + 5.67628\left(\frac{N}{M_N}\right)^2 - 47.0895$ for $3.727 \le \frac{N}{M_N} \le 4.538$; $G_N = 0$, for $\frac{N}{M_N} < 3.727$ or $\frac{N}{M_N} > 4.538$ (This sets the limits for the N integral).

$$F(N, E_{Kc}) = \frac{P_{Kc}E_{Kc}}{(2\pi)^4\hbar^6}\left\{1 - \frac{2(M_Y^2+M_N^2)}{(N-E_{Kc})^2-P_{Kc}^2} + \left[\frac{M_Y^2-M_N^2}{(N-E_{Kc})^2-P_{Kc}^2}\right]^2\right\}^{\frac{1}{2}}\left\{3(N-E_{Kc})^2\left(1-\left[\frac{M_Y^2-M_N^2}{(N-E_{Kc})^2-P_{Kc}^2}\right]^2\right) - P_{Kc}^2\left(1 - \frac{2(M_Y^2+M_N^2)}{(N-E_{Kc})^2-P_{Kc}^2} + \left[\frac{M_Y^2-M_N^2}{(N-E_{Kc})^2-P_{Kc}^2}\right]^2\right)\right\}.$$ (Interchange Y and K for $F(N, E_{Yc})$)

$P_{Uc} = \left[E_{Uc}^2 - M_U^2\right]^{\frac{1}{2}}$; $\beta_{Uc} = \frac{P_{Uc}}{E_{Uc}}$; $\cot\theta_{U\ell} = \bar\gamma(\cot\theta_{Uc} + \frac{\bar\beta}{\beta_{Uc}}\csc\theta_{Uc})$; $\bar\gamma = \frac{E_{T\ell}}{N} = 8.53\left(\frac{M_N}{N}\right)$; $\bar\beta = \left[1 - (\bar\gamma)^{-2}\right]^{\frac{1}{2}}$;

$\gamma_{U\ell}(1-\beta_{U\ell}\cos\Theta_\ell) = M_U^{-1}\left\{\bar\gamma(E_{Uc} + \bar\beta P_{Uc}\cos\theta_{Uc}) - P_{Uc}\sin\theta_{Uc}\cos\phi_{Uc}\right\}$; $\frac{4\pi}{k+1} = \int_{\theta_{Uc}=0}^{\pi}\int_{\phi_{Uc}=0}^{2\pi}\cos^k\theta_{Uc}\sin\theta_{Uc}\, d\phi_{Uc}\, d\theta_{Uc}$, for k even.

C. Tables to be Given

Sets of a_1, a_2; r_1, r_2; $\Delta\Omega_{\gamma\ell}$, i (beam-intensity weighting factor) for summation over target, slit subdivisions;

$\int_0^{E_{\gamma\ell}^{max}} \epsilon(E_{\gamma\ell})\, dE_{\gamma\ell}$: (in Mev)

E	∫	E	∫	E	∫	E	∫	E	∫	E	∫	E	∫	E	∫
0	0	100	1.80	200	17.14	300	45.54	400	81.90	500	123.40	600	168.26	700	215.64
20	0	120	3.48	220	22.00	320	52.28	420	89.86	520	132.14	620	177.56	720	225.34
40	0	140	5.90	240	27.30	340	59.30	440	98.00	540	141.00	640	186.96	740	235.12
60	0.18	160	9.04	260	33.00	360	66.60	460	106.32	560	149.98	660	196.44	760	244.96
80	0.74	180	12.80	280	39.10	380	74.14	480	114.78	580	159.06	680	206.00	780	254.86

D. Constants

Fixed

$c = 2.998 \times 10^{10}$ cm/sec

$M_N = 939$ Mev

$M_{\pi^0} = 135$ Mev

Change with change in decay scheme

$N+N \rightarrow N+K^0+ \begin{matrix}\Lambda\\ \Sigma\end{matrix}$ $K^0 \rightarrow \pi^0+\pi^0$	$N+N \rightarrow N+K^\pm+ \begin{matrix}\Lambda\\ \Sigma\end{matrix}$ $K^\pm \rightarrow \pi^\pm+\pi^0$	$N+N \rightarrow N+\Lambda^0+K$ $\Lambda^0 \rightarrow N+\pi^0$	$N+N \rightarrow N+\Sigma^+ +K$ $\Sigma^+ \rightarrow P+\pi^0$
$M_U = 497.8$ Mev	$M_U = 494$ Mev	$M_U = 1115.2$ Mev	$M_U = 1189.4$ Mev
$M_Y = \begin{matrix}1115.2\\ 1189.4\end{matrix}$ Mev	$M_Y = \begin{matrix}1115.2\\ 1189.4\end{matrix}$ Mev	$M_K = 494$ Mev	$M_K = 494$ Mev
$\tau_U = 0.95 \times 10^{-10}$ sec	$\tau_U = 1.22 \times 10^{-8}$ sec	$\tau_U = 2.77 \times 10^{-10}$ sec	$\tau_U = 0.83 \times 10^{-10}$ sec
$n = 4$	$n = 2$	$n = 2$	$n = 2$
$\beta_{\pi^0\mu} = 0.8400$	$\beta_{\pi^0\mu} = 0.8373$	$\beta_{\pi^0\mu} = 0.6084$	$\beta_{\pi^0\mu} = 0.8139$
$\gamma_{\pi^0\mu} = 1.843$	$\gamma_{\pi^0\mu} = 1.829$	$\gamma_{\pi^0\mu} = 1.260$	$\gamma_{\pi^0\mu} = 1.721$

Change within decay scheme

j = integer

k = integer

a_{jk} = weighting factor for sets of j, k (not shown explicitly above, deduced by empirical fit)

E. Limits

$E_{Y\ell}$

$$E_{Y\ell}^{min} = \frac{\gamma_{\pi^0\mu} M_{\pi^0}(1-\beta_{\pi^0\mu})}{2\gamma_{U\ell}(1-\beta_{U\ell}\cos\theta_\ell)}$$

$$E_{Y\ell}^{max} = \frac{\gamma_{\pi^0\mu} M_{\pi^0}(1+\beta_{\pi^0\mu})}{2\gamma_{U\ell}(1-\beta_{U\ell}\cos\theta_\ell)}$$

E_{Uc}

$$E_{Uc}^{min} = M_U$$

$$E_{Kc}^{max} = (N^2 - [M_N + M_Y]^2 + M_K^2)/2N$$

Interchange Y and K for E_{Yc}^{max}

ϕ_U

Two ranges

Range 1: $0 \le \theta_{U\ell} \le \frac{\pi}{2}$ $\sin\phi_U^{min} = \tan\alpha_1 \cot\theta_{U\ell}$; for $\sin < 0$, > 1, $\int d\phi = 0$

or $\sin\phi_U^{max} = \tan\alpha_2 \cot\theta_{U\ell}$; for $\sin < 0$, > 1, $\phi_U^{max} = \frac{\pi}{2}$

$\frac{\pi}{2} \le \theta_{U\ell} \le \pi$ $\sin\phi_U^{min} = \tan\alpha_2 \cot\theta_{U\ell}$; for $\sin < 0$, > 1, $\int d\phi = 0$

$\sin\phi_U^{max} = \tan\alpha_1 \cot\theta_{U\ell}$; for $\sin < 0$, > 1, $\phi_U^{max} = \frac{\pi}{2}$

Range 2: $\phi_2^{min} = \pi - \phi_1^{max}$; $\phi_2^{max} = \pi - \phi_1^{min}$

θ_{Uc}

$$\ell_\pm(\theta_{U\ell}) = \cot^{-1}\left[\frac{\cot\theta_{U\ell} \pm \frac{\bar\beta}{\beta_{Uc}}[\cot^2\theta_{U\ell} + \bar\gamma^2(1-\frac{\bar\beta^2}{\beta_{Uc}^2})]^{\frac{1}{2}}}{\bar\gamma\,(1-\frac{\bar\beta^2}{\beta_{Uc}^2})}\right]$$

	$\beta_{Uc} > \bar\beta$		$\beta_{Uc} \le \bar\beta$ †	
	θ_{Uc}^{min}	θ_{Uc}^{max}	θ_{Uc}^{min}	θ_{Uc}^{max}
$0 \le \alpha_1 < \alpha_2 \le \frac{\pi}{2}$	$\ell_-(\alpha_1)$	$\ell_-(\pi/2)$	$\ell_-(\alpha_1)$*	$\ell_+(\alpha_1)$
$0 \le \alpha_1 \le \frac{\pi}{2} \le \alpha_2 \le \pi$	$\ell_-(\alpha_1)$	$\ell_-(\alpha_2)$	$\ell_-(\alpha_1)$*	$\ell_+(\alpha_1)$
$\frac{\pi}{2} \le \alpha_1 < \alpha_2 \le \pi$	$\ell_-(\pi/2)$	$\ell_-(\alpha_2)$	*	*

†For $\beta_{Uc} \le \bar\beta$ and $\theta_{Uc} \ge \cos^{-1}(-\frac{\beta_{Uc}}{\bar\beta})$ use ℓ_+; otherwise use ℓ_-.

*$\cot^2\theta_{U\ell} \le \bar\gamma^2(1-\frac{\bar\beta^2}{\beta_{Uc}^2}) \Rightarrow \int d\theta = 0$.

REFERENCES

1. Bjorklund, Crandall, Moyer, and York, Phys. Rev. 77, 213 (1950).
2. Richard L. Garwin, Phys. Rev. 90, 274 (1953).
3. Balandin, Balashov, Zhukov, Pontecorvo, and Selivanov, J. Exptl. Theoret. Phys. (U. S. S. R.) 29, 265 (1955).
4. Ridgeway, Berley, and Collins, Phys. Rev. 104, 513 (1956).
5. D. Berley and G. B. Collins, Bull. Am. Phys. Soc., Series II, 1, 320 (1956).
6. D. Berley and G. B. Collins, Phys. Rev. 112, 614 (1958).
7. John E. Osher, π^0 Modes of Heavy-Meson and Hyperon Decay (Thesis), UCRL-3449, June 1956.
8. Osher, Moyer, and Parker, Bull. Am. Phys. Soc., Series II, 1, 185 (1956).
9. Osher, Moyer, and Parker, A Study of θ_1^0 Production and Decay by Observation of Its Neutral Decay Mode, UCRL-8429, July 1958.
10. Michiyuki Nakamura, Multiple Coincidence and Anticoincidence Circuit, UCRL Counting Note No. CC3-1, 1956.
11. W. Heitler, The Quantum Theory of Radiation, Third Edition (Oxford Press, London, 1954). (Complete except for screening correction which is given in Rossi.[12])
12. Bruno Rossi, High-Energy Particles, (Prentice-Hall, New York, 1952).
13. For a list of references on experiments relating to the cross-section, see Donald W. Barr, Nuclear Reactions of Copper Induced by 5, 7-Bev Protons, UCRL3793, May 1957.
14. Lester Winsberg, University of California Radiation Laboratory, private communication, 1959.
15. D. C. Peaslee, Phys. Rev. 105, 1034 (1957).
16. Saul Barshay, Phys. Rev. 104, 853 (1956).
17. Julian Schwinger, Interactions of the Fundamental Particles, Notes on Lectures by J. Schwinger, Harvard, 1956 (Prepared by L. S. Rodberg).
18. Block, Harth, and Sternheimer, Phys. Rev. 100, 324 (1955).
19. J. V. Lepore and M. Neuman, A Statistical Model for High-Energy Events, UCRL-2649, July 1954.